ASTROBIOLOGY
Volume 18, Number 3, 2018
Mary Ann Liebert, Inc.
DOI: 10.1089/ast.2017.1666

Organic Haze as a Biosignature in Anoxic Earth-like Atmospheres

Giada Arney,[1,2] Shawn D. Domagal-Goldman,[1,2] and Victoria S. Meadows[2,3,4]

Abstract

Early Earth may have hosted a biologically mediated global organic haze during the Archean eon (3.8–2.5 billion years ago). This haze would have significantly impacted multiple aspects of our planet, including its potential for habitability and its spectral appearance. Here, we model worlds with Archean-like levels of carbon dioxide orbiting the ancient Sun and an M4V dwarf (GJ 876) and show that organic haze formation requires methane fluxes consistent with estimated Earth-like biological production rates. On planets with high fluxes of biogenic organic sulfur gases (CS_2, OCS, CH_3SH, and CH_3SCH_3), photochemistry involving these gases can drive haze formation at lower CH_4/CO_2 ratios than methane photochemistry alone. For a planet orbiting the Sun, at 30× the modern organic sulfur gas flux, haze forms at a CH_4/CO_2 ratio 20% lower than at 1× the modern organic sulfur flux. For a planet orbiting the M4V star, the impact of organic sulfur gases is more pronounced: at 1× the modern Earth organic sulfur flux, a substantial haze forms at $CH_4/CO_2 \sim 0.2$, but at 30× the organic sulfur flux, the CH_4/CO_2 ratio needed to form haze decreases by a full order of magnitude. Detection of haze at an anomalously low CH_4/CO_2 ratio could suggest the influence of these biogenic sulfur gases and therefore imply biological activity on an exoplanet. When these organic sulfur gases are not readily detectable in the spectrum of an Earth-like exoplanet, the thick organic haze they can help produce creates a very strong absorption feature at UV-blue wavelengths detectable in reflected light at a spectral resolution as low as 10. In direct imaging, constraining CH_4 and CO_2 concentrations will require higher spectral resolution, and $R > 170$ is needed to accurately resolve the structure of the CO_2 feature at 1.57 μm, likely the most accessible CO_2 feature on an Archean-like exoplanet. Key Words: Organic haze—Organic sulfur gases—Biosignatures—Archean Earth. Astrobiology 18, 311–329.

1. Introduction

The Archean eon (3.8–2.5 billion years ago) may have experienced several intervals when a transient organic haze globally veiled our planet (*e.g.* Trainer *et al.*, 2006; Zerkle *et al.*, 2012; Izon *et al.*, 2015, 2017; Hicks *et al.*, 2016). This haze would have dramatically altered our planet's climate, spectral appearance, and photochemistry (Pavlov *et al.*, 2001a, 2001b; Domagal-Goldman *et al.*, 2008; Haqq-Misra *et al.*, 2008; Wolf and Toon, 2010; Hasenkopf *et al.*, 2011; Kurzweil *et al.*, 2013; Claire *et al.*, 2014; Arney *et al.*, 2016, 2017). Organic haze formation is driven by methane photochemistry, and its optical thickness is controlled by the ratio of the amount of atmospheric methane (CH_4) relative to the amount of carbon dioxide (CO_2) (*e.g.,* Trainer *et al.*, 2006) because oxygen radicals produced by CO_2 photolysis can frustrate organic haze formation in Earth-like atmospheres (Arney *et al.*, 2017).

On Archean Earth, there are numerous potential sources of methane, although biological processes likely dominated, as they do today (Kharecha *et al.*, 2005). Methanogenesis, an anaerobic metabolism deeply rooted in the tree of life that likely evolved early in Earth's history (Woese and Fox, 1977; Ueno *et al.*, 2006), involves the uptake of CO_2 and H_2 to form CH_4 and H_2O:

$$CO_2 + 4H_2 \rightarrow CH_4 + 2H_2O$$

Methanogenesis has only been observed in types of archaea, and it occurs in a number of anoxic environments on

[1]NASA Goddard Space Flight Center, Greenbelt, Maryland.
[2]NASA Astrobiology Institute Virtual Planetary Laboratory, University of Washington, Seattle, Washington.
[3]Astronomy Department, University of Washington, Seattle, Washington
[4]University of Washington Astrobiology Program, Seattle, Washington.

modern Earth including animal guts and hydrothermal vents (Ver Eecke *et al.*, 2012). In the latter environment, methanogens react H_2 contained in reduced vent fluids with CO_2 dissolved in the seawater. On Earth today, the flux of methane produced by biology is roughly 10^{11} molecules/cm^2/s (Pavlov *et al.*, 2001a), and the Archean biotic flux has been estimated to range somewhere between 1/3 and 2.5 times this modern value (Kharecha *et al.*, 2005).

The abiotic production rate of methane is not as well constrained. Serpentinization, the hydration of olivine and pyroxene, is the dominant abiotic source of methane on Earth today (Kelley *et al.*, 2005; Etiope and Sherwood Lollar, 2013; Guzmán-Marmolejo *et al.*, 2013). The source of methane from serpentinizing systems is not completely clear. Serpentinization produces H_2, and it has been suggested that this H_2 can then react with CO_2 or CO to form CH_4 through Fischer-Tropsch-type reactions (Bradley and Summons, 2010). However, other explanations for methane produced in serpentinizing systems have been offered. For example, methanogens are known to live in these systems, so some fraction of the methane produced from the vents is biological (Brazelton *et al.*, 2006). However, based on the total density of cells expected in the vent systems, it is unlikely that methanogens are the dominant methane source in at least the Lost City hydrothermal system (Bradley and Summons, 2010). More recently, the isotopic composition of the hydrocarbons emanating from the Von Damm hydrothermal system was analyzed in relation to the isotopic composition of dissolved inorganic carbon (McDermott *et al.*, 2015). Surprisingly, the isotopic composition of the vented CH_4 indicates that little to none of the CH_4 coming out the Van Damm vents is produced by reduction of dissolved inorganic carbon circulating through the rocks and participating in Fischer-Tropsch-type chemistry. Possibly, the CH_4 produced in these systems is released from trapped magmatic fluid inclusions. Consistent with this finding, McCollom (2016) conducted laboratory experiments on the serpentinization of olivine with and without pyroxene using ^{13}C-labeled CO_2 and found that production rates of $^{13}CH_4$ were inefficient. ^{13}C-labeled CH_4 was produced in only one of their experiments: this experiment also contained a dissolved H_2-rich vapor phase that may help promote Fischer-Tropsch-type reactions. The kinetic barriers to methane formation in these reactions are surmountable in the presence of iron-nickel-phase mineral catalysts such as awaurite, although the McDermott *et al.* (2015) study of the Von Damm vent implies that at least in some serpentinizing systems these reactions are not important for the bulk methane production and another source dominates.

Kasting and Catling (2003) estimated the abiotic flux of methane as 1/300th the biotic rate. However, more recent measurements by Kelley *et al.* (2005) at the Lost City hydrothermal system indicate that abiotic methane production rates may actually be as high as 1/30th the biotic flux.

A different line of argument to estimate the abiotic methane production from serpentinization on Earth comes from Guzmán-Marmolejo *et al.* (2013). These authors calculate how much methane can be produced given current crustal spreading rates as a function of available FeO in the crust and by considering CO_2 as the limiting reactant for methane production in serpentinization—however, note that if the CH_4 is instead produced by a different mechanism, this assumption may no longer apply. Based on the assumption of Fischer-Tropsch-type synthesis, they estimate that the maximum amount of abiotic methane that can be produced from serpentinization is 6.8×10^8 molecules/cm^2/s for a 1-Earth-mass planet, which is only 1/160th the biotic flux (Guzmán-Marmolejo *et al.* [2013] also estimate the maximum CH_4 production rate as 1.3×10^9 molecules/cm^2/s for a 5-Earth-mass planet). However, note that these results are contingent on the assumption of the modern-day Earth crustal spreading rate and the source of the methane.

Considering all the above estimates, abiotic methane production estimates from serpentinization ranging between approximately 1/30th and 1/150th the present biotic flux appear reasonable for modern Earth. In the Archean, abiotic methane production rates are even less certain than they are today. If the early planet had faster seafloor spreading rates or a higher fraction of seafloor ultramafic rocks, enhanced abiotic methane compared to the modern planet would have been possible (Kasting, 2005; Shaw, 2008). Faster seafloor spreading rates may be more likely on a hotter young planet where convection may have proceeded more efficiently. How tectonics operated in the Archean remains uncertain, but there is geological and numerical modeling evidence supporting the existence of plate tectonics during this period (Kerrich and Polat, 2006).

Although serpentinization is thought to be the dominant source of abiotic methane on Earth today, there are other abiotic methane sources (Etiope and Sherwood Lollar, 2013). These sources include primordial delivery (via exogeneous sources); internal magmatic, postmagmatic, and metamorphic processes; iron-carbonate decomposition; carbonate methanation; and aqueous CO_2 reduction. Global emissions of all non-anthropogenic biotic methane fluxes to the atmosphere have been well studied and constrained at approximately 200 Mt/year (Core Writing Team *et al.*, 2007). Total estimated methane emissions from geological sources amount to about 60 Mt/year (about 1×10^{10} molecules/cm^2/s), although this flux is probably not purely abiotic (Etiope, 2012): Etiope and Sherwood Lollar (2013) discuss how volcanic and nonvolcanic geothermal systems can also release methane derived from thermal breakdown of sedimentary rock organic matter, which can be biotic (Etiope *et al.*, 2007). The total global emission of truly abiotic methane is not well constrained. Emmanuel and Ague (2007) suggest it may be as low as $\sim$2.3 Mt/year (about 4×10^8 molecules/cm^2/s), although Etiope and Sherwood Lollar (2013) point out that this estimate is hypothetical and not has not been constrained by direct measurements. Of course, we emphasize again that all these estimates are for modern-day Earth; past Earth, and other planets, will naturally have different methane flux rates.

Given all of this, finding an organic haze in the atmosphere of a planet with Archean-like CO_2 levels could be indicative of highly interesting processes that imply ongoing geological activity and/or biological methane production with high methane source fluxes to drive haze production in a CO_2-rich atmosphere. Such a planet should be a target of closer follow-up studies aimed at discriminating between geological and biological CH_4 sources and to search for other signs of habitability and life (Section 4.3). We emphasize that while detection of CH_4 and organic haze—which can have a significantly stronger spectral signature than CH_4—in an Earth-like atmosphere would be a tantalizing hint of the presence of methane-producing life on an exoplanet (since biology produces the bulk of methane on modern Earth), it would not be enough to conclude biological activity given the existence of abiotic CH_4 sources. This is similar to—but perhaps more obvious than—the case for oxygen as a biosignature given that several pathways for abiotic oxygen production have recently come to light (Domagal-Goldman *et al.*, 2014; Harman *et al.*, 2015; Luger and Barnes, 2015; Schwieterman *et al.*, 2016). The spectral signatures of possibly biologically produced spectral features need to be placed in the context of a broader understanding of that planet's atmospheric chemistry and potential for habitability. In this manuscript, we pursue one type of contextual information that would help to discriminate between abiotic and biotic hazes on Earth-like worlds.

It has been pointed out that biogenic organic sulfur gases (S_{org}) can contribute to the atmospheric hydrocarbon budget through photochemical processes that liberate organic species from the S_{org} molecules (Domagal-Goldman *et al.*, 2011). These S_{org} gases include carbon disulfide (CS_2), carbonyl sulfide (OCS), methanethiol (CH_3SH, also called methyl mercaptan), and dimethyl sulfide (CH_3SCH_3 or DMS). Volcanic processes can also produce CS_2 and OCS, but at lower fluxes than Earth's biology (Lomans *et al.*, 2002). The potential for S_{org} gases to act as biosignatures has been considered by previous studies (Pilcher, 2003; Vance *et al.*, 2011), and Domagal-Goldman *et al.* (2011) showed that although S_{org} gases may be difficult to directly detect in a planet's spectrum, their photochemical byproducts can produce spectral signatures that can indirectly imply a flux of these gases. In particular, Domagal-Goldman *et al.* (2011) found the photolysis of S_{org} gases can release methyl radicals (CH_3) that contribute to ethane (C_2H_6) production in excess of the amount predicted from methane photochemistry alone. This effect is especially pronounced around M dwarfs whose UV spectral output allows for longer atmospheric lifetimes of C_2H_6 than solar-type stars. Unfortunately, C_2H_6 absorbs most strongly in the mid-IR at 12 μm, making its detection potentially difficult. Domagal-Goldman *et al.* (2011) did not consider S_{org}-rich atmospheres with enough methane to lead to haze formation, nor did they simulate the spectral region in which hazes have detectable features. But the same principles that caused higher C_2H_6 in their simulations could also cause a greater haze concentration in the presence of S_{org}. Here, we will test whether the hydrocarbons contributed to the atmosphere by S_{org} photochemistry can induce haze formation at lower CH_4/CO_2 ratios than would be expected if haze formation was driven by methane production alone, thereby providing a spectral clue that biological activities may be influencing haze formation on a planet. Organic haze is a particularly useful potential biosignature because it produces a very strong broadband absorption feature at UV and visible wavelengths (this is the reason why Titan is orange), and it also produces absorption features in the near infrared (NIR). These features may be accessible with observatories becoming available in the coming decades, including the James Webb Space Telescope (JWST) and possible future large direct-imaging telescopes such as the Large UV Optical Infrared telescope (LUVOIR) and the Habitable Exoplanet Imaging Mission (HabEx) (Postman *et al.*, 2010; Bolcar *et al.*, 2015; Dalcanton *et al.*, 2015; Mennesson *et al.*, 2016), as we have studied previously (Arney *et al.*, 2017).

2. Methods

To simulate Archean-analog planets, we use a coupled 1D photochemical-climate model called Atmos. The Atmos model is described in detail in Arney *et al.* (2016), and limitations of the Atmos haze formation scheme are discussed in Arney *et al.* (2016) and Arney *et al.* (2017). In brief, this model assumes a pathway proposed for Titan's hazes (Allen *et al.*, 1980; Yung *et al.*, 1984) where haze formation occurs via polymerization of acetylene (C_2H_2). In this scheme, haze particles are formed via $C_2H + C_2H_2 \rightarrow C_4H_2$ and $C_2H + CH_2CCH_2 \rightarrow C_5H_4 + H$. However, Cassini measurements of Titan show that haze formation is more complex and includes ion chemistry and the formation of nitriles (Waite *et al.*, 2007; Vuitton *et al.*, 2009; López-Puertas *et al.*, 2013). Additionally, while Titan's atmosphere is extremely reducing, Archean Earth's atmosphere would have been less so, and laboratory studies have shown that oxygen atoms can be incorporated into haze molecules (Trainer *et al.*, 2006; DeWitt *et al.*, 2009; Hörst and Tolbert, 2014; Hicks *et al.*, 2016). Lack of these processes in Atmos may cause the model to underpredict the haze formation rate; on the other hand, in a real atmosphere, C_4H_2 would be able to revert back to C_2H_2. Our model does not include this, which could lead to haze overprediction. Ongoing improvements to Atmos will include a more complete haze formation scheme.

The climate portion of Atmos was originally developed by Kasting and Ackerman (1986), although it has been significantly modernized since then, and it was most recently updated and described in a recalculation of habitable zone boundaries around main sequence stars (Kopparapu *et al.*, 2013) and in a study of the impact of organic haze in the Archean (Arney *et al.*, 2016). The photochemical portion of Atmos is based on a code developed by Kasting *et al.* (1979), and it was significantly modernized by Zahnle *et al.* (2006). This model, supported by the Virtual Planetary Laboratory in NASA's Astrobiology Institute, is now publicly available at https://github.com/VirtualPlanetaryLaboratory/atmos.

The climate model is considered converged when the change in flux out the top of the atmosphere and change in surface temperature are sufficiently small (typically on the order of 1×10^{-5}) and when the energy from the star into the atmosphere balances the energy radiated out of the atmosphere. The photochemical model uses a first-order reverse Euler solver to solve continuity and flux equations for each species at all altitudes. In the time-stepping loop, the model tracks how much the gas concentrations change in each step, and the species with the largest relative error in its change in concentration (called E_{max}) is used to set the size of the next time step. When E_{max} is small, the next time step will be larger; if E_{max} is too large, the model will decrease the time-step size. The model checks the time-step length to determine convergence, and when the time-step size exceeds 1×10^{17} s, the model considers itself ''converged'' and stops.

Both the climate and photochemical models have been modified to simulate haze particles as fractal in shape rather than as spherical (Mie) particles (Wolf and Toon, 2010; Zerkle *et al.*, 2012; Arney *et al.*, 2016) by using the fractal mean field approximation (Botet *et al.*, 1997). Studies of Titan's atmosphere indicate that fractal particles are more realistic for organic hazes (Rannou *et al.*, 1997), and early Earth–analog fractal organic hazes have been simulated in the laboratory (Trainer *et al.*, 2006). Zerkle *et al.* (2012) and Arney *et al.* (2016) describe our model's haze particle treatment in detail. Fractal particles are composed of multiple smaller spherical particles called monomers clumped together into complex branching forms, and their scattering and absorption physics differ from spherical particles. In general, compared to equal-mass spherical particles, fractal particles produce more extinction at shorter wavelengths and less extinction at longer wavelengths. The consequences of this behavior have been previously considered in the context of UV-shielding and climate cooling effects for an Archean haze (Wolf and Toon, 2010; Zerkle *et al.*, 2012; Arney *et al.*, 2016). Generally, haze particles initially form at altitudes of 80–90 km; this altitude is a result of the model's photochemistry and is not prescribed.

The methyl radicals produced by S_{org} gases that participate in haze formation photochemistry can be generated by reactions such as

$$CH_3SH + O \rightarrow CH_3 + HSO \quad (1)$$

$$CH_3SH + h\nu \rightarrow CH_3 + HS \quad (2)$$

The full chemical network that S_{org} gases participate in is discussed in detail in Domagal-Goldman *et al.* (2011). Once CH_3 is produced, it directly contributes to haze formation via the process outlined in Arney *et al.* (2017): CH_3 produces ethane most efficiently through CH_3 + $CH_3CO \rightarrow C_2H_6 + CO$. Ethane can then be photolyzed to produce C_2H_4 or C_2H_2, or it can react with OH to produce C_2H_5, all of which step toward haze formation.

Spectra are generated by the Spectral Mapping Atmospheric Radiative Transfer model (SMART) (Meadows and Crisp, 1996; Crisp, 1997) using outputs from the Atmos model. SMART is a 1D, line-by-line, fully multiple scattering radiative transfer model. Haze is included in SMART from Atmos via a particle binning scheme described in Arney *et al.* (2016). The newest version of SMART can also calculate transit transmission spectra in the same model run that calculates reflected light spectra. The model's transit calculations include the path length and refraction effects inherent in transit transmission spectra (Misra *et al.*, 2014a, 2014b).

To simulate observations with possible large future space-based telescopes, we use the coronagraph noise model described in Robinson *et al.* (2016). The same nominal parameters are assumed as those discussed in Robinson *et al.,* except we assume a telescope operating temperature of 270 K and a constant quantum efficiency as a function of wavelength (0.9). Noise sources include dark noise, read noise, zodiacal and exozodiacal light, stellar light leakage, telescope thermal radiation. A publically accessible online version of this simulator is available at https://asd.gsfc.nasa.gov/luvoir/tools.

2.1. Model inputs

We compare haze production under the influence of S_{org} gases for planets orbiting the Sun 2.7 billion years ago (Ga) during the Archean eon and the M4V dwarf GJ 876 with the same total insolation as the 2.7 Ga Sun (0.8×1360 W/m^2). GJ 876 is a known multiplanet host (Von Braun *et al.*, 2014). The spectrum we use for it is described in Domagal-Goldman *et al.* (2014) based on the spectrum reported in France *et al.* (2012). We chose this star over higher-activity M dwarfs (*e.g.,* AD Leo) because Domagal-Goldman *et al.* (2011) showed that S_{org} gases have a greater impact on hydrocarbon photochemistry for lower-activity M dwarfs. Stars with lower UV outputs generate fewer photochemical oxygen species, which are major sinks of both hydrocarbons and organic sulfur gases (Domagal-Goldman *et al.*, 2011; Arney *et al.*, 2017). For the Sun, we corrected its spectrum for higher levels of expected activity when it was younger using the wavelength-dependent solar evolution correction from Claire *et al.* (2012), which estimates the solar flux at different epochs by combining data from the Sun and solar analogues to determine appropriate wavelength-dependent stellar flux corrections. The stellar spectra used in this study are shown for the UV, visible, and NIR in Fig. 1. The UV spectra shown in Fig. 1 show the actual resolution of the wavelength grid used by the photochemical model. The model's ''Lyman alpha'' bin encompasses flux from wavelengths spanning 8 Å wide on either side of Lyman alpha (121.6 nm).

Our chemical reaction network is based on the one used by Arney *et al.* (2016) and Arney *et al.* (2017), although these earlier studies did not include S_{org} gases. The supplementary online information of Arney *et al.* (2016) provides a complete list of chemical reactions and species boundary conditions for this nominal Archean model. To

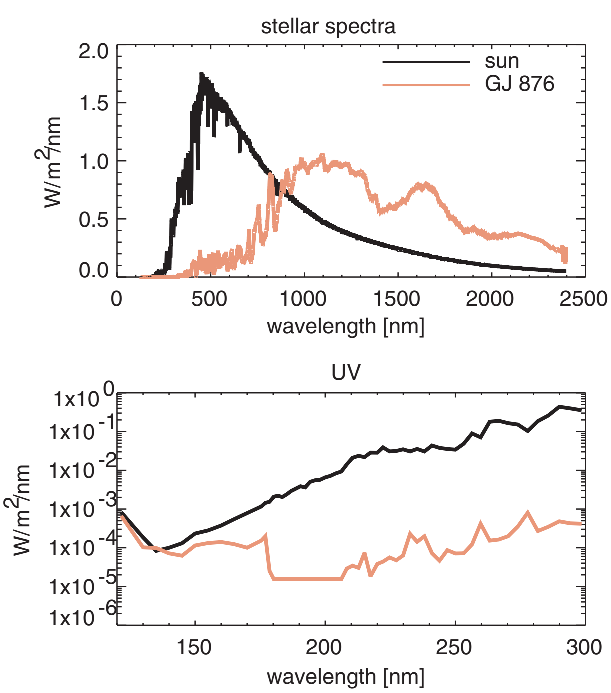

FIG. 1. Spectra of the Archean Sun and GJ 876 used in this study. The bottom panel shows the actual UV wavelength grid used in the photochemical model. Wavelength bins are larger than individual emission lines (*e.g.,* Lyman alpha).

include S_{org}, we updated our templates based on the reaction list and boundary conditions discussed in Domagal-Goldman *et al.* (2011). However, we removed the NH_3-related gases and reactions from the templates shown in Domagal-Goldman *et al.* (2011) because we have not yet incorporated NH_3 into our climate model, and it is a potentially significant greenhouse gas. Inclusion of NH_3 remains an important area of future work because it may play a role in warming our early planet under the fainter young Sun, especially under a haze that could protect it from UV photolysis (Sagan and Chyba, 1997; Pavlov *et al.*, 2001a; Wolf and Toon, 2010). Our atmospheres with 1× S_{org} fluxes use the same S_{org} surface boundary fluxes presented in Table 2 of Domagal-Goldman *et al.* (2011). In units of molecules/cm^2/s, these fluxes are 1.4×10^7 for CS_2 and OCS, 8.3×10^8 for CH_3SH, 4.2×10^9 for CH_3SCH_3, and 0 for $CH_3S_2CH_3$. This last species, $CH_3S_2CH_3$, or dimethyl disulfide (DMDS), is not produced by biology but results from S_{org} photochemistry. Other nonbiological S_{org} gases relevant to S_{org} photochemistry included in our photochemical scheme are CS (1.7×10^7 molecules/cm^2/s produced at the surface), and CH_3S (0 molecules/cm^2/s produced at the surface, but photochemistry can produce this gas in the atmosphere).

Unlike our previous studies where we set the CH_4 surface mixing ratio to explore haze formation under different CH_4 concentrations (Arney *et al.*, 2016, 2017), here we vary the CH_4 surface flux and allow the photochemical model to calculate the self-consistent atmospheric mixing ratio from the selected fluxes to explore haze formation under different CH_4 production rates. The CO_2 atmospheric fractions ($f$$CO_2$) simulated here range from 1×10^{-5} to 1×10^{-1}; the lower limit on CO_2 abundance was chosen to roughly represent the limit for C4 photosynthesis (Kestler *et al.*, 1975; Tolbert *et al.*, 1995), which is determined by the ability of plant stomata to maintain a diffusive gradient of CO_2 concentration from the atmosphere into the cellular structure. Estimates of Archean CO_2 have ranged from values close to those of modern Earth to orders of magnitude higher (*e.g.,* Rosing *et al.*, 2010; Dauphas and Kasting, 2011; Driese *et al.*, 2011; Kanzaki and Murakami, 2015); in our previous work (Arney *et al.*, 2016, 2017), we adopted the values from Driese *et al.* (2011) for our nominal estimates of pCO_2 at 2.7 Ga (pCO_2 $\sim 1\times10^{-3}$ to 1×10^{-2} bar). Here, we choose an upper limit on CO_2 that is an order of magnitude larger than the Driese *et al.* (2011) range. Note that organic haze formation in a much more oxidizing atmosphere (such as Mars-like with 95% CO_2 or modern day Earth-like with its 21% O_2) is not tenable at any plausible hydrocarbon production rates. For significantly more reducing atmospheres than those shown here (*i.e.,* Titan-like), haze formation can be possible at very low methane source fluxes compared to the ones we simulate, which would make an argument for biological involvement in methane production difficult. In this study, methane surface fluxes were chosen to range between 6.8×10^8 to 1×10^{12} molecules/cm^2/s. The lower limit on methane production is taken from the theoretical study of abiotic, serpentinization-driven methane production by Guzmán-Marmolejo *et al.* (2013) for Earth-like worlds. Life on Earth produces CH_4 at a rate of $\sim 1\times10^{11}$ molecules/cm^2/s, and the upper limit for methane flux we consider is an order of magnitude larger than this amount.

For haze optical properties, we use the optical constants of Khare *et al.* (1984) subject to the caveats outlined in Arney *et al.* (2016), where we discuss how these optical constants were derived for Titan-analog (not Archean-analog) hazes. However, Archean-simulant haze optical constants have only been measured at one wavelength (532 nm) by a previous study (Hasenkopf *et al.*, 2010), and the Khare *et al.* (1984) haze measurements agree reasonably well with the Hasenkopf *et al.* (2010) measurement. We are currently involved with laboratory work to simulate and measure new optical constants for Archean-analog organic hazes from the UV to the NIR, but haze production rates are slow in CO_2-rich conditions, and the analyses will not be ready in time for inclusion in this manuscript. However, we will use these updated optical constants in the future and make them publically available once we do.

We assume a total surface pressure of 1 bar for all simulations. The background atmosphere is composed of N_2. When we refer to CH_4/CO_2 ratios, note that we are referring to the value at the surface since CH_4 does not follow an isoprofile in these atmospheres. CO_2, meanwhile, is assumed to be well mixed. We set molecular oxygen (O_2) at a mixing ratio of 1×10^{-8}, corresponding to a time after the origin of oxygenic photosynthesis but before substantial oxygen accumulation in the atmosphere (Kharecha *et al.*, 2005; Claire *et al.*, 2014). Note that haze can form at higher oxygen concentrations than considered here and possibly even at oxygen concentrations corresponding to the low Proterozoic O_2 levels suggested by Planavsky *et al.* (2014) of 0.1% the present atmospheric level as shown by Kurzweil *et al.* (2013) and Izon *et al.* (2017). However, haze can only form in such atmospheres at CH_4 fluxes higher than those we consider here.

To generate spectra, we use the HITRAN 2012 linelists (Rothman *et al.*, 2013) and set a solar zenith angle of 60°, which approximates the flux observed at quadrature. As in Atmos, optical constants for the haze particles in SMART are derived from the Khare *et al.* (1984) optical constants using the fractal mean field approximation.

3. Results

In this section, we consider haze as a biosignature in the context of atmospheres with and without S_{org} gases.

As a baseline case, we first consider haze formation in the absence of biogenic sulfur gases to explore how varying CO_2 and CH_4 levels affects haze production. Figure 2 shows the optical thickness of an organic haze in the atmosphere of an Archean planet with no S_{org} orbiting the ancient (2.7 Ga) Sun, and Fig. 3 shows the same for an Archean-analog planet orbiting GJ 876. In these contour plots, optical depth of unity at 190 nm (chosen to represent hazes that would significantly impact photochemistry and the planet's spectrum) is marked with the solid black lines overlying the colored contours. Figures 2 and 3 show that lower CH_4 fluxes are needed to form optically thick hazes for the simulated planets around GJ 876 compared to the planets simulated around the ancient Sun. This is consistent with our findings in Arney *et al.* (2017), which showed that lower CH_4/CO_2 ratios are required to form hazes around Archean-analog worlds orbiting GJ 876, because this star's lower UV output generates fewer haze-destroying oxygen radicals

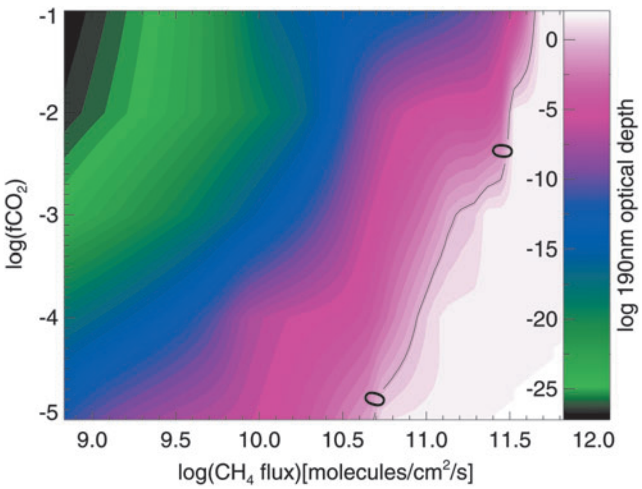

FIG. 2. The colored contours show the log optical depth of the Archean haze (for a planet orbiting the Sun) at 190 nm as a function of the log atmospheric fraction of CO_2, log(fCO_2), on the vertical axis, and the log of the CH_4 surface flux on the horizontal axis. Haze optical depth of unity (log(1) = 0) is marked by the solid black line.

from processes like CO_2 photolysis. At the Driese *et al.* (2011) CO_2 levels, haze production requires methane fluxes broadly consistent with estimated Archean biological methane production rates (~ 0.3–$2.5 \times 1 \times 10^{11}$ molecules/cm^2/s) according to Kharecha *et al.* (2005). This is the case for both simulations of a planet orbiting the Archean Sun and simulations of a planet orbiting GJ 876.

In Figs. 4–7, we include S_{org} fluxes to show how this additional source of hydrocarbons affects haze formation. Figures 4 and 6 are analogous to Figs. 2 and 3 for the Sun and GJ 876, respectively. In the gray region of Figs. 6 and 7, simulations are not converged; in this part of parameter space, very thick hazes generated extreme stratospheric heating ($\sim$400 K), causing model instabilities. In Figs. 5 and 7, we show the same data, but here the horizontal axis shows the CH_4/CO_2 ratio instead of the CH_4 flux for two reasons. First, this emphasizes how the presence of significant S_{org} fluxes can impact the CH_4/CO_2 ratio required to form haze. Second, these plots show the actual spectral observables since it is the CH_4 mixing ratio—not its flux—that can be observed from a spectrum (the latter could only be inferred through modeling once the concentrations of atmospheric gases—and the UV spectrum of the star—were measured). In all four figures of simulations including S_{org} fluxes (Figs. 4–7), the top panel corresponds to the optical depth contours for 1× the modern S_{org} fluxes as defined in Domagal-Goldman *et al.* (2011), and the bottom panel corresponds to 30× the modern S_{org} fluxes, chosen for consistency with the upper limit for the S_{org} flux value in Domagal-Goldman *et al.* (2011). In both panels, the solid red line denotes where the haze's 190 nm optical depth equals unity for 1× S_{org}, and the solid black line denotes where the haze optical depth is unity for 30× S_{org}. These lines are plotted together in both panels so that they can be easily compared.

Figures 5 and 7 show that as fCO_2 decreases, the CH_4/CO_2 ratio required to form a thick haze increases. This result is counter-intuitive and arises because the total carbon budget of the atmosphere decreases as CO_2 is removed; in other words, any given atmosphere has less CH_4 available to form haze at a fixed CH_4/CO_2 ratio at lower CO_2 levels. More significantly, when fluxes of S_{org} increase, the CH_4/CO_2 ratio necessary to form a haze decreases at all CO_2 levels for planets orbiting both stars. This occurs because photochemistry readily forms methyl groups from organic sulfur gases, and formation of CH_3 is a step in the haze formation process. By increasing the efficiency of these processes, the CH_4/CO_2 ratio required to form haze at a given CO_2 concentration is lowered.

For a solar-type star with 1× S_{org}, Fig. 4 shows the CH_4 fluxes required to form haze are similar to the simulations with no S_{org}. However, in the presence of 30× S_{org}, the CH_4 fluxes required to initiate haze formation decrease by about 50% for the highest CO_2 level considered ($fCO_2 = 10^{-1}$) and by almost an order of magnitude for $fCO_2 = 10^{-3}$. Figure 5 shows that at $fCO_2 = 10^{-2}$, the CH_4/CO_2 ratio needed to form a haze for the planet around the solar-type star with τ (190 nm) = 1 at 190 nm is about 0.2 for the 1× S_{org} case. This is roughly the same as the CH_4/CO_2 ratio required to form a substantial haze in the absence of S_{org} (Arney *et al.*, 2016). For the 30× S_{org} case, the CH_4/CO_2 ratio required to form substantial haze for the same planet with $fCO_2 = 10^{-2}$ is about 0.16, a 20% decrease.

Around GJ 876, S_{org} has a larger impact on haze formation with markedly less methane required to form an optically thick haze at high S_{org} fluxes. In Fig. 6, at $fCO_2 = 10^{-2}$, the haze becomes optically thick at over an order of magnitude smaller CH_4 fluxes in the presence of 30× S_{org} compared to 1× S_{org}. Figure 7 shows that at 1× S_{org}, the haze becomes optically thick at slightly less than $CH_4/CO_2 = 0.2$, but for 30× S_{org}, the haze becomes optically thick at $CH_4/CO_2 \sim 0.02$, a full order of magnitude lower. As discussed above, haze forms more readily in the atmosphere of the GJ 876 planet because GJ 876's spectrum results in the production of a smaller quantity of haze-destroying oxygen radicals from CO_2 photolysis compared similar planets orbiting the Sun (Arney *et al.*, 2017).

Figures 5 and 7 show that for planets around both stars, as fCO_2 decreases (and, therefore, as the absolute amount of

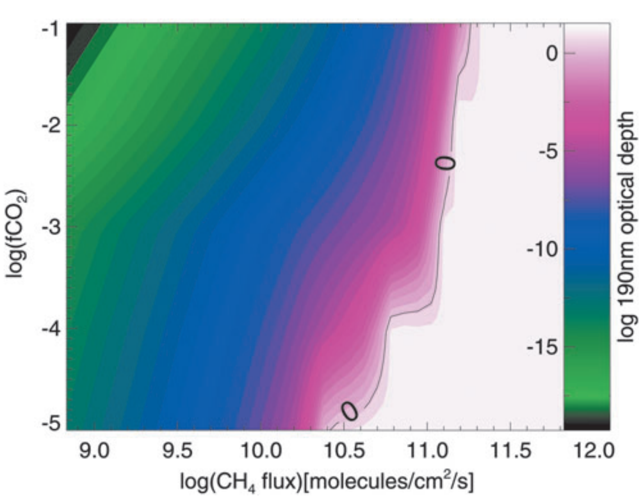

FIG. 3. Same as Fig. 3 but for an Archean-analog planet orbiting GJ 876.

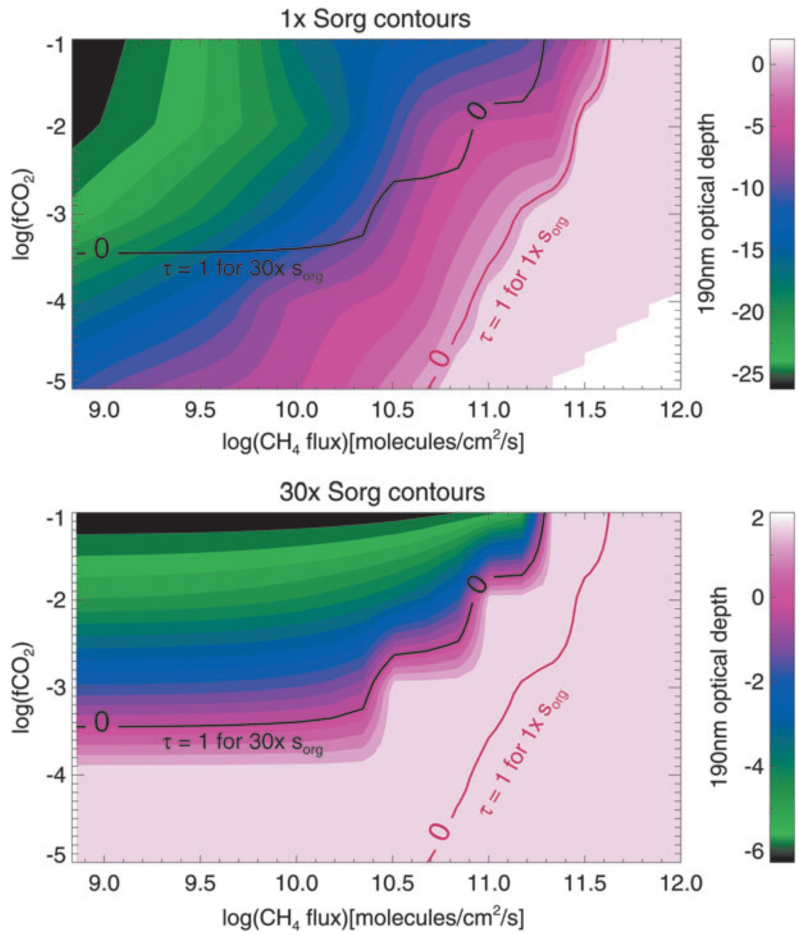

FIG. 4. The log of the 190 nm optical depth of organic haze for planets around the Sun at 1× S_{org} and 30× S_{org} as a function of log(f-CO_2) and surface CH_4 flux. The red line in both panels shows where optical depth is unity for 1× S_{org}, and the black line in both panels shows where optical depth is unity for 30× S_{org}. The 1× and 30× S_{org} optical depth of unity lines are overlain over the contours on both panels so that they may be easily compared.

CH_4 in the atmosphere at a given CH_4/CO_2 ratio also decreases), the difference between the CH_4/CO_2 ratios required to form a thick haze with 1× S_{org} versus 30× S_{org} increases because S_{org} becomes a larger proportional contributor to the atmosphere's hydrocarbon budget.

Interestingly, S_{org} gases themselves provide enough hydrocarbons to not only affect haze formation but also affect the absolute methane abundance. For example, for a planet around the Sun with a methane flux of 1×10^{11} molecules/cm^2/s and $fCO_2 = 1\times10^{-2}$, we find that an atmosphere without S_{org} gases generates a surface methane mixing ratio of 2.2×10^{-4}, while an atmosphere with 30× S_{org} gases generates a surface methane mixing ratio of 6.8×10^{-4}. Around GJ 876, the same planets have surface methane mixing ratios of 6.7×10^{-4} and 7.3×10^{-3} for no S_{org} and 30× S_{org}, respectively. The largest photochemical sources of CH_4 in the 30× S_{org} atmospheres are $CH_3 + HCO \rightarrow CH_4 + CO$ and $CH_3 + H \rightarrow CH_4$. These reactions occur 1–2 orders of magnitude faster in the 30× S_{org} atmospheres due to the production of S_{org}-derived methyl radicals. Although the high S_{org} atmospheres have higher methane levels, which itself allows haze to form more readily, Figs. 5 and 7 show clearly that the hazes in the high-S_{org} atmospheres still form at lower methane mixing ratios than they would without S_{org} gases because the S_{org} gases also contribute other gases relevant to haze formation (*e.g.,* CH_3 and C_2H_6). The methane derived from S_{org} gases also imposes a lower limit on the amount of methane in these high S_{org} atmospheres. For instance, the lowest CH_4/CO_2 ratios generated in our 30× S_{org} simulations (bottom panels of Figs. 5 and 7) are higher than the lowest CH_4/CO_2 ratios for 1× S_{org} (top panels of Figs. 5 and 7).

4. Discussion

Haze formation in atmospheres with Archean-like levels of CO_2 can indicate methane production rates consistent with known and theoretical Earth-like biogenic methane production rates, and these fluxes are higher than known and theoretical rates of abiotic methane production on modern Earth. However, more efficient abiotic methane production rates on early Earth and exoplanets cannot be ruled out. Thus, while haze would not be definitive proof of life on these planets, it would indicate that they are consistent with the behavior of Earth's methanogenic biosphere and therefore are highly interesting targets for follow-on studies. We have shown here that detecting an organic haze in the presence of a relatively low CH_4/CO_2 ratio could further imply the influence of biogenic sulfur gases aiding haze formation. This is similar to the suggestion of ethane as a spectral biosignature in Domagal-Goldman *et al.* (2011), as photolysis of methyl-bearing S_{org} gases enhances formation of ethane in atmospheres with large S_{org} fluxes even if the S_{org} gases themselves are difficult to detect directly. The impact of S_{org} on haze formation is more pronounced around M dwarf stars like GJ 876 because the lower overall UV flux

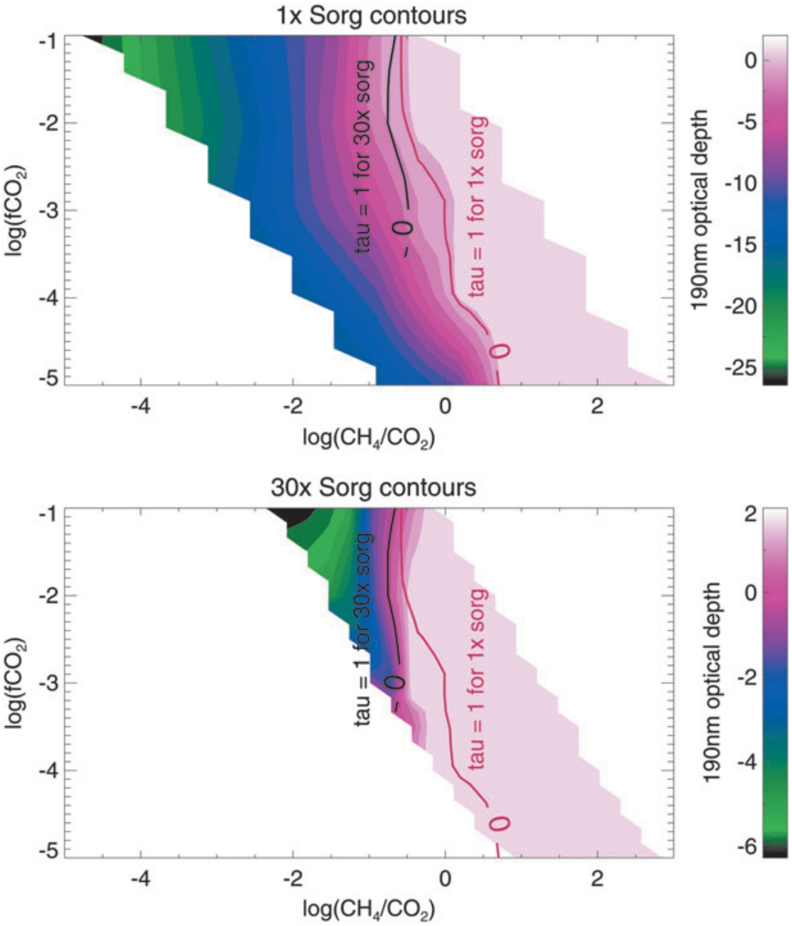

FIG. 5. Same as Fig. 4 but showing the log of the 190 nm optical depth of organic haze for planets around the Sun at 1× S_{org} and 30× S_{org} as a function of log(fCO$_2$) and log(CH_4/CO_2).

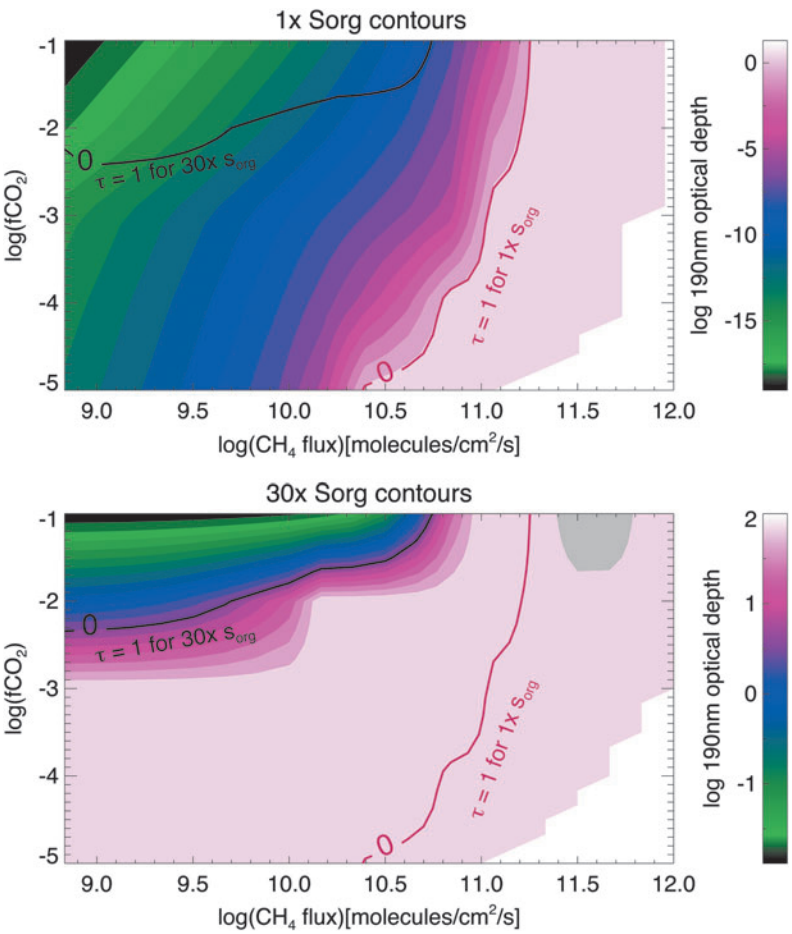

FIG. 6. Same as Fig. 4 but for planets orbiting GJ 876. Simulations in the gray region are not converged.

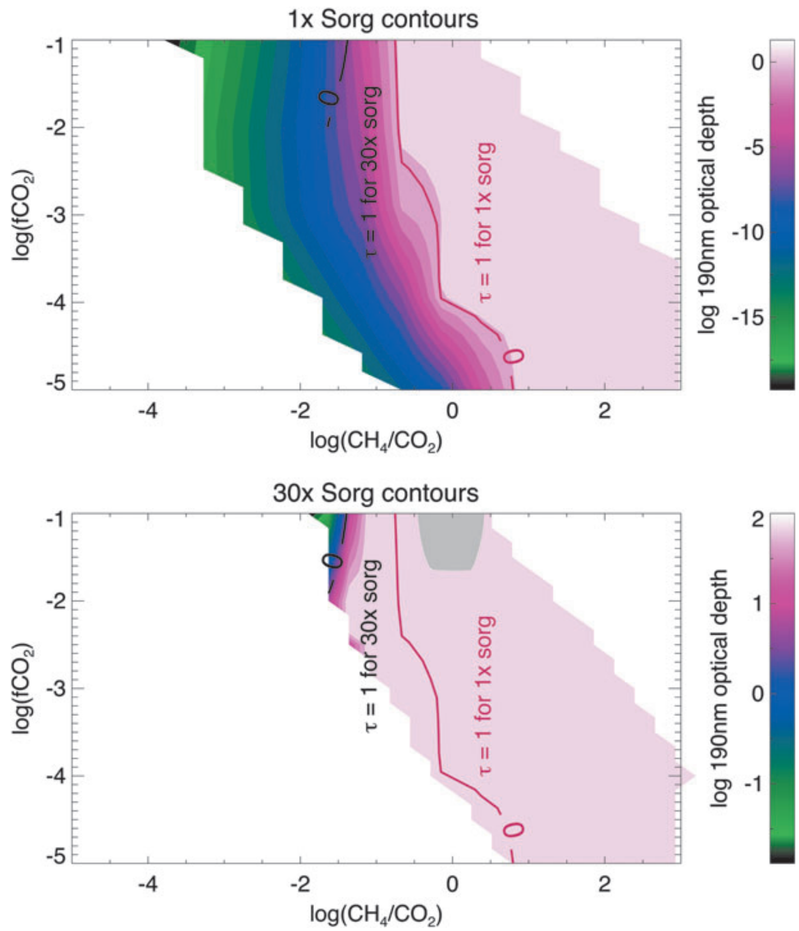

FIG. 7. Same as Fig. 5 but for planets orbiting GJ 876.

around this star leads to smaller sinks of hydrocarbon gases (Domagal-Goldman *et al.*, 2011; Arney *et al.*, 2017).

In all situations—including planets without S_{org} gases—it will be important to know the redox state and temperature regime of an atmosphere to argue for the plausible biogenicity of an organic haze. Titan shows us that abiotic hazes can form in highly reducing cold atmospheres with long residence lifetimes for methane. Estimating the temperature of a planet will require measurements of the planet's semimajor axis and greenhouse gas budget. However, the temperature difference between Titan and early Earth is large—about 200 K—and so only broad temperature constraints would be needed to separate Titan-like planets from Earth-like planets. To understand the atmospheric redox state of a given world, measurements of CO_2 and CH_4 will be required to constrain the CH_4/CO_2 ratio. Additional discussion on the interpretation of a haze spectral feature in the context of the rest of the planetary environment can be found in Section 4.3.

4.1. Detectability considerations

Transit observations with JWST (Beichman *et al.*, 2014) could provide access to NIR wavelengths on hazy exo-Earths and were discussed in detail by Arney *et al.* (2017). Planets orbiting M dwarfs are more amenable to observations with JWST compared to planets around solar-type stars due to the larger planet-to-star size ratio and more frequent transits for planets in the habitable zone. In Fig. 8 we show the transit transmission spectra of hazy Archean Earth with 1× and 30× S_{org} around the Sun and GJ 876 to illustrate which spectral features may be detectable for these worlds. The planets shown around the Sun-like star were simulated with a methane flux of 6.9×10^{10} molecules/cm^2/s and a CO_2 mixing ratio of 1×10^{-3}, corresponding to surface methane mixing ratios of 7.9×10^{-5} and 3.2×10^{-4} for 1× and 30× S_{org}, respectively. The planets around the GJ 876–like star were simulated with a methane flux of 3.1×10^{10} molecules/cm^2/s and a CO_2 mixing ratio of 1×10^{-2}, with resultant surface methane mixing ratios of 1.4×10^{-4} and 1.2×10^{-3}. These atmospheres were chosen to represent cases where haze is not significantly present at 1× S_{org} but is present at 30× S_{org}. As expected, Fig. 8 shows that the spectral consequences of high S_{org} fluxes are more significant for the planet orbiting GJ 876.

Even at 30× S_{org}, organic sulfur gases are not apparent in the transit transmission spectrum. Domagal-Goldman *et al.* (2011) showed that these S_{org} gases are concentrated in the lower atmosphere since they are readily photolyzed at higher layers, so they are spectrally inaccessible at the altitudes probed by transits for a hazy planet (20–80 km for the planets in Fig. 8). Haze, CH_4, CO_2, and C_2H_6 are all potentially detectable, however. Organic haze could be discerned through the presence of a haze-induced NIR spectral slope, and haze produces an absorption feature near 6 μm and a much weaker one near 3 μm (not labeled). CH_4 absorbs near 1.1, 1.4, 1.7,

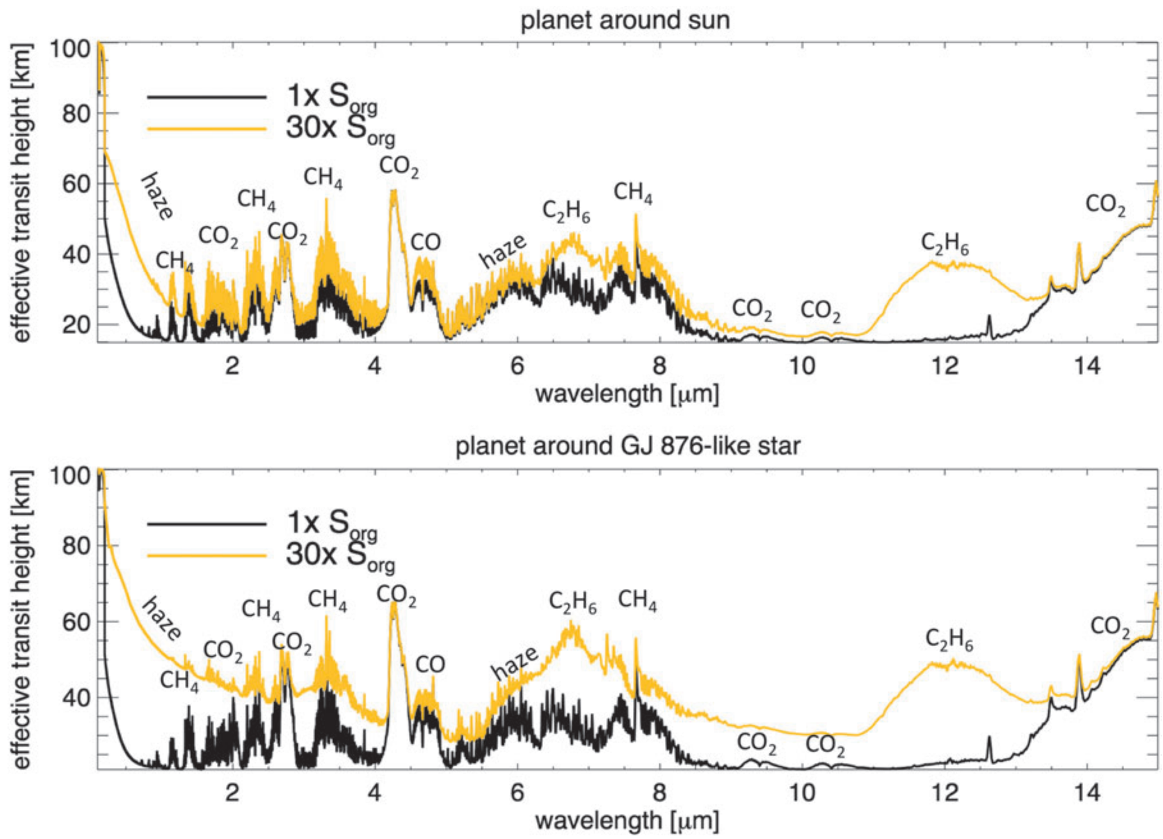

FIG. 8. Representative transit transmission spectra of Archean Earth-like planes with different S_{org} fluxes. The *y* axis shows the effective tangent height, which is the altitude above the planet's surface that light on tangent transit path lengths can penetrate into the atmosphere. Spectra are shown for $\Delta\lambda = 0.01\ \mu m$.

2.3, 3.3, and 7.5 μm. CO_2 also absorbs at wavelengths accessible to JWST at 1.57, 2, 2.7, and 4.3 μm. C_2H_6 produces features near 6.5 and 12 μm. The features at wavelengths longward of about 8 μm can probably be considered inaccessible to JWST due to the dim stellar blackbody at these wavelengths. See Arney *et al.* (2017) for our discussion of how observable these features are with JWST for a planet orbiting a star like GJ 876.

Potential direct imaging telescopes under consideration such as LUVOIR and HabEx may provide direct observations of Earth-like exoplanets in the 2030s and beyond (Postman *et al.*, 2010; Bolcar *et al.*, 2015; Dalcanton *et al.*, 2015; Stapelfeldt *et al.*, 2015; Mennesson *et al.*, 2016). Figure 9 shows the reflected light spectra of the same planets shown in Fig. 8. Haze produces a broad, deep spectral feature at UV-blue wavelengths; for this combination of CH_4-CO_2-S_{org}, the haze feature is weaker for the planet around the Sun-like star compared to the planet around the GJ 876–like star, but it still significantly alters the shape of the spectrum at wavelengths <0.5 μm. This very strong feature is the reason why we argue here that haze is likely a much more detectable indicator of atmospheres with S_{org} compared to the C_2H_6 discussed in Domagal-Goldman *et al.* (2011) that absorbs in the mid-IR. Of course, for both transit transmission and direct imaging observations, how well we will be able to determine whether a haze is present at an anomalously low CH_4/CO_2 ratio depends on how well we will be able to retrieve the CH_4 and CO_2 gas concentrations.

To examine the spectral resolutions ($R = \lambda/\Delta\lambda$) required to observe features in hazy reflected light spectra, Fig. 10 shows the reflectance spectrum of a representative hazy Archean Earth at several spectral resolutions for $fCO_2 = 10^{-2}$ and $CH_4/CO_2 = 0.2$. The Fig. 10 spectrum includes water clouds added to our 1D radiative transfer model by using a weighted averaging technique where 50% of the planet is considered haze-covered and cloud-free, 25% is covered by haze and stratocumulus clouds, and 25% is covered by cirrus clouds and haze (Robinson *et al.*, 2011). Haze produces a broad, strong absorption feature at short wavelengths that can be easily resolved at spectral resolutions as low as 10. Methane and CO_2 are observable in the NIR, although CO_2 is more challenging to detect. Carbon dioxide has features near 1.57 and 2 μm for the wavelengths shown here, but telescope thermal emission could swamp the 2 μm feature for a noncryogenically cooled mirror. Therefore, the most detectable CO_2 feature in reflected light occurs at 1.57 μm for Archean-like CO_2 levels. Resolving the narrow multipeaked structures of the 1.57 μm CO_2 feature will require spectral resolution $R > 100$, and $R > 170$ will be required to correctly resolve the depths of the narrow bands of this feature. As in the transit transmission spectrum, S_{org} features are not detectable in the reflected light spectrum.

Although there are numerous interesting spectral features in the NIR, they may not be detectable in direct imaging observations even if telescopic thermal emission is negligible because inner working angle (IWA) constraints alone can limit access to longer wavelengths. The IWA represents the smallest

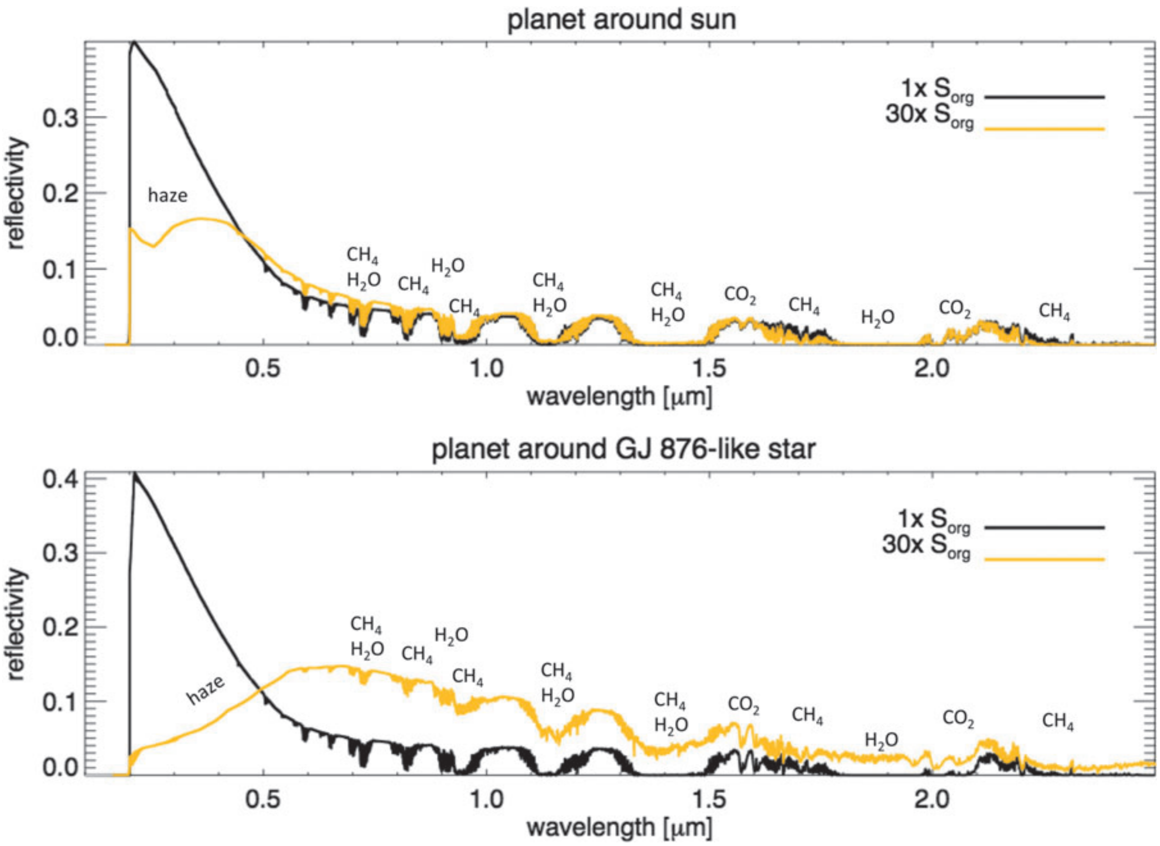

FIG. 9. Representative reflected light spectra of Archean Earth-like planes with different S_{org} amounts for the same atmospheres shown in Fig. 8. These spectra do not include water clouds to show the spectral impact of only organic haze.

planet-star angular separation that can be resolved with sufficient signal-to-noise to detect the planet. For a coronagraph, the IWA scales with $C \times \lambda/D$, where C is a small valued-constant of order unity and D is the telescope diameter. Several mirror diameters are being considered for the designs of the HabEx and LUVOIR mission concepts. Currently, these designs include a 4 m monolith (HabEx), a JWST-sized 6.5 m mirror (HabEx), a 9.2 m mirror (LUVOIR), and a 15.1 m mirror (LUVOIR). Note, however, that light reflected off the jagged hexagonal segments on the outside of a segmented mirror poses a challenge for current coronagraph designs. Therefore, to be conservative, we will consider only light reflected from the largest inscribed circle that fits within each segmented aperture, resulting in a smaller effective aperture visible to the coronagraph. For the segmented telescope sizes listed previously, these correspond to inscribed diameters of 5.5, 7.6, and 12.7 m, respectively, for the current designs of these telescopes (M. Bolcar, personal communication).

To receive an Archean-like level of instellation (*i.e.,* stellar irradiation), a planet orbiting a star like GJ 876 would be at a planet-star separation distance of 0.12 AU. Assuming an optimistic IWA of λ/D and a 12.7 m aperture, a GJ 876–like planet-star system could be located no farther away than 4.5 pc for the IWA to allow characterization of the spectrum out to 1.57 μm to see the CO_2 band using a coronagraph. Smaller telescopes fare worse, as does assuming more conservative IWAs such as IWA = 2 λ/D or IWA = 3 λ/D. Table 1 shows the longest wavelength observable before the IWA cuts off the spectrum for planet-star systems located at a fixed distance of 4.5 pc assuming a solar-type star and a GJ 876–type star for the four different telescope sizes being studied by HabEx and LUVOIR (with the IWAs for the segmented telescopes use their inscribed circle diameters). At 4.5 pc, it is difficult to characterize the planet orbiting GJ 876 in the NIR unless the telescope is the largest we simulate and/or the IWA is the most optimistic we consider. The influence of S_{org} on haze formation is most pronounced around M dwarfs like GJ 876, but as we have seen, IWA constraints make Earth-like planets around such stars more challenging to characterize since they orbit so close to their host stars. Note, however, that here we are assuming that starlight suppression is achieved with a coronagraph, but star shades may be able to provide smaller IWAs than those discussed here, depending on star-shade size and star shade–telescope separation distance (Turnbull *et al.*, 2012).

Figure 11 shows the integration times required to obtain a signal-to-noise ratio (SNR) of 20 as a function of wavelength for planets with the same hazy Archean atmospheric parameters used to generate Fig. 10 by using the Robinson *et al.* (2016) coronagraph noise model. We assume $R = 170$ in the visible and NIR to fully resolve the structure of the narrow 1.57 μm CO_2 band peaks and troughs, and $R = 20$ in the UV (for $\lambda < 0.4$ μm). Vertical lines indicate IWA cutoffs as described in the figure caption. We again assume apertures of 4, 5.5, 7.6, and 12.7 m, and the planet-star system is assumed to be 4.5 pc to allow detection of the 1.57 μm CO_2 band for a planet orbiting a star like GJ 876 with IWA = λ/D for the largest telescope. We chose to simulate SNR = 20

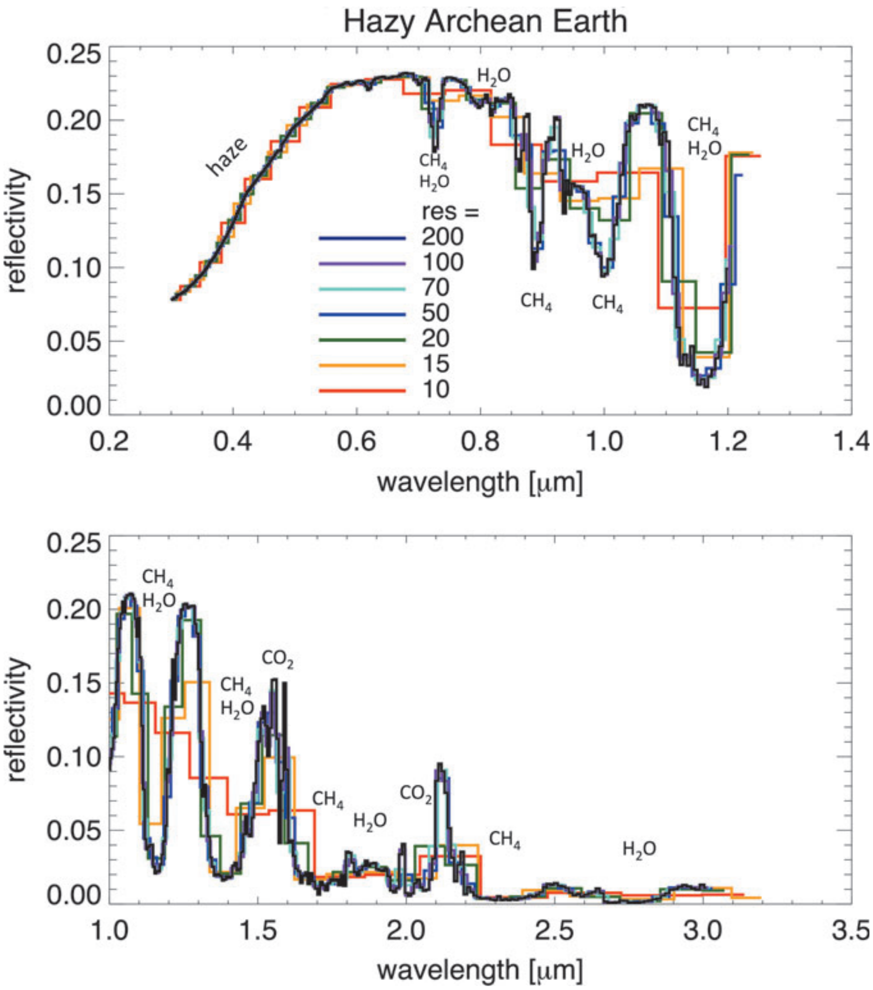

FIG. 10. The reflected light spectra of hazy Archean Earth at several spectroscopic resolutions. The haze absorption feature at $\lambda < 0.6\,\mu m$ is sufficiently strong and broad to be resolved at very low spectral resolution. These spectra include water clouds in addition to haze, via a weighted averaging technique in our 1D model (50% haze only, 25% haze and cirrus cloud, and 25% haze and stratocumulus cloud).

because studies have shown that continuum SNR measurements of about 20 may be required to constrain gas abundances in planetary atmospheres (Lupu *et al.*, 2016; Nayak *et al.*, 2017; M. Marley, personal communication). Note in Fig. 11 that absorption bands, where the planet is darker, require longer integration times to reach SNR = 20, but the gas retrieval demands discussed above apply to the continuum regions, where the planet is brighter. Because M dwarfs are dimmer than Sun-like stars in the visible, longer integration times are required to characterize the planet around GJ 876 at wavelengths <1 μm compared to the planet orbiting the Sun. The situation is reversed for wavelengths >1 μm. The dramatic increase in integration times near 1.6 μm is caused by the telescope's thermal emission (the mirror is 270 K), rendering these longer wavelengths effectively unobservable for a noncryogenic telescope even if they were accessible within the IWA wavelength cutoff.

Integration times at all wavelengths increase by at least an order of magnitude for the 4 m telescope compared to the 12.7 m telescope. For the 12.7 m telescope, sensing continuum regions to a level of SNR = 20 would generally require tens to hundreds of hours of observing time for the resolution shown here. For the 4 m telescope, measuring the continuum at SNR = 20 demands hundreds to thousands of hours of integration.

4.2. Other hydrocarbon-containing gases

Although we included just S_{org} gases in our photochemical model, there are numerous other methyl-containing

Table 1. Wavelength Cutoffs for Four Mirror Diameters and Three IWAs for Planet-Star Systems at 4.5 pc

Mirror diameter (m)	*Cutoff for IWA = λ/D (μm)*		*Cutoff for IWA = 2 λ/D (μm)*		*Cutoff for IWA = 3 λ/D (μm)*	
	GJ 876	*Sun*	*GJ 876*	*Sun*	*GJ 876*	*Sun*
12.7	1.6	14	0.82	6.8	0.54	4.6
7.6	0.98	8.2	0.49	4.1	0.33	2.7
5.5	0.71	6.0	0.36	3.0	0.24	2.0
4	0.52	4.3	0.26	2.2	0.17	1.4

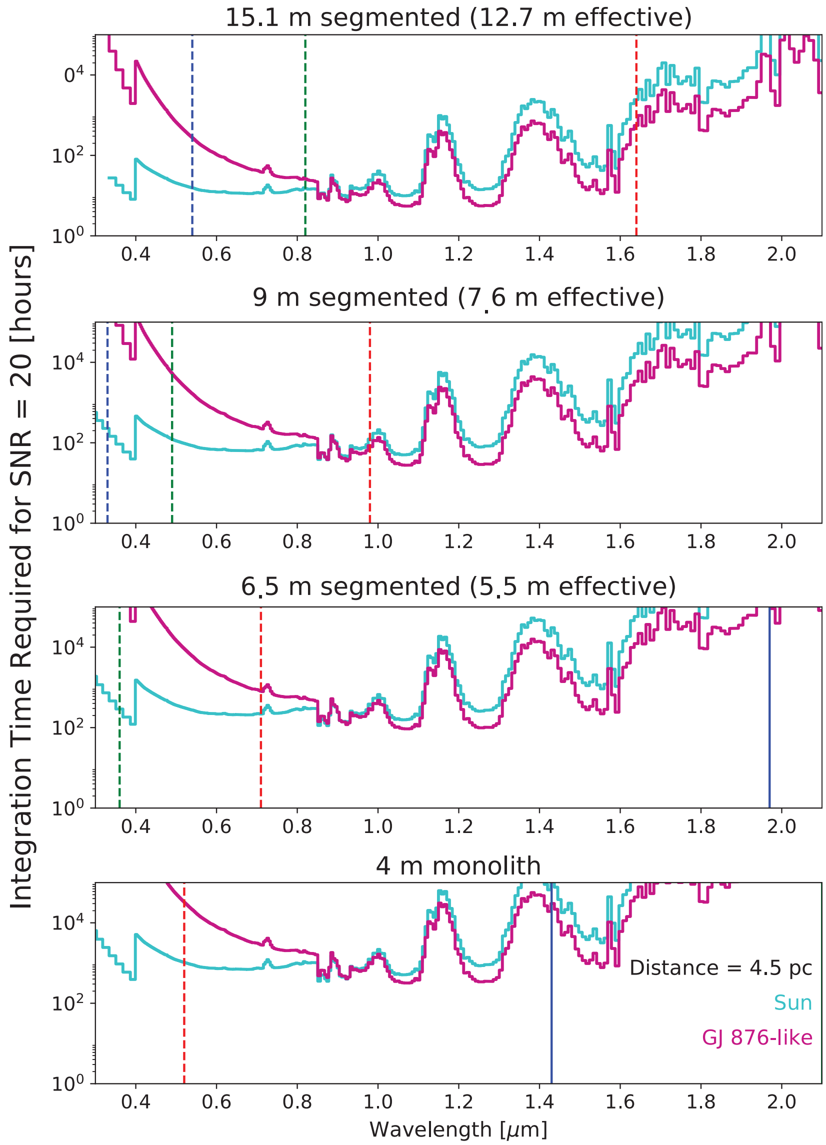

FIG. 11. The wavelength-dependent integration time required to obtain a SNR = 20 for hazy Archean-analog planets orbiting the Sun and GJ 876 at 4.5 pc as observed by four different telescope architectures. The red, green, and blue vertical lines represent the wavelength cutoffs for IWA = λ/*D*, 2 λ/*D*, and 3 λ/*D*, respectively. The dashed lines are the IWA cutoffs for a GJ 876–like star, and the solid lines represent the IWA cutoffs for a solar-type star. Not all IWA cutoffs are shown on every plot if they do not overlap with the wavelength range displayed: for instance, all the solar IWA lines occur redward of the right axis of the 12.7 and 7.6 m plots. The discontinuity at 0.4 and 0.85 μm is due to the boundary between the assumed UV, visible, and NIR detectors.

gases produced by terrestrial organisms and other processes (Seager *et al.*, 2012) that may contribute to photochemical organic haze production if present in a planet's atmosphere. Such gases include CH_3Cl (methyl chloride), CH_3Br (methyl bromide), CH_3I (methyl iodide), CH_3OH (methanol), and terpenes. Methyl chloride, in particular, has been shown in a previous study to have a longer photochemical lifetime in the atmospheres of Earth-like planets orbiting M dwarfs compared to Sun-like stars (Segura *et al.*, 2005), though note that the other methyl-containing compounds listed here were not tested in the Segura *et al.* study. Natural sources of methyl chloride, the most abundant halocarbon in the atmosphere (Yokouchi *et al.*, 2000), include oceanic sources (Koppmann *et al.*, 1993) such as planktonic algae (Harper *et al.*, 2003), plants (Yokouchi *et al.*, 2000; Rhew, 2011), and biomass burning (Blake *et al.*, 1996). Higher-order halogenated organic compounds such as C_2H_4Cl, C_3H_7Cl, and C_4H_9Cl, as well as methyl chloride itself, can also be produced in soils and sediments when chlorine ions are alkylated through organic matter oxidation (Keppler *et al.*, 2000). An overview of methyl chloride sources, including industrial ones, is provided in Keppler *et al.* (2005). Non-anthropogenic sources of methyl bromide include marine algae and biomass burning (Blake *et al.*, 1996; McCauley *et al.*, 1999), kelp (Manley and Dastoor, 1988), other oceanic sources (Anbar *et al.*, 1996), and plants (Rhew, 2011). Methyl iodide can be produced by vegetation and soils (Sive *et al.*, 2007), oceanic sources (Rasmussen *et al.*, 1982) including kelp and microbial metabolisms (Manley and Dastoor, 1988), and biomass burning (Blake *et al.*, 1996). Methanol is the simplest alcohol and is produced by a variety of anaerobic metabolisms including methanotrophy (Xin *et al.*, 2004). In the atmosphere, it can contribute to the tropospheric HOx budget after being oxidized to formaldehyde (Solomon *et al.*, 2005). Terpenes are a broad class of organic compounds released by plants and insects (Pare and Tumlinson, 1999) that are responsible for atmospheric phenomena such as the low-lying blue haze that can be seen over some forested regions like the Blue Ridge Mountains (Went, 1960). Some terpenes such as d-limonene can ultimately generate gases like formaldehyde and formic acid in the atmosphere through photochemical processing (Walser *et al.*, 2007).

The largest potential fluxes of these gases would likely be on planets where they are the by-product of metabolism. On modern Earth, major sources of these gases (including CH_3SH) are typically the degradation of amino acids (Stoner *et al.*, 1994; Lomans *et al.*, 2002). However, on planets with a different atmospheric composition, there might be an energetic incentive to produce these gases directly. The potential for this has been demonstrated in the laboratory, in experiments where methanogens are given H_2S as a substrate in place of H_2, and in response produce CH_3SH instead of CH_4 (Moran *et al.*, 2008). On a planet with globally high H_2S concentrations, microbes could release high fluxes of CH_3SH to the atmosphere, accumulating CH_3SH and its photochemical by-products (C_2H_6 in particular) to potentially detectable levels (Domagal-Goldman *et al.*, 2011). Other atmospheric compositions may also lead to an incentive for other gases to be produced. For example, an atmosphere rich in halogens—and HCl, HI, and HBr in particular—may incentivize the biological production of CH_3Cl, CH_3I, and CH_3Br. While this has not been studied in the laboratory, nor modeled in a photochemical simulation, this sort of atmosphere would create the largest concentration of—and therefore spectral signal from—these gases.

Such gases have been considered in the context of atmospheric biosignatures since they are produced by biological processes (Seager *et al.*, 2012), although as we have seen here and in Domagal-Goldman *et al.* (2011), photochemistry and the strength of these gases' spectral signatures will determine whether they—or any of their photochemical by-products—are useful gases (or aerosols) to target in the search for life beyond Earth. For instance, the spectral signatures of CH_3Cl were investigated in Segura *et al.* (2005) in simulations that included photochemistry. CH_3Cl was readily destroyed by the solar spectrum for a planet orbiting the Sun, but for planets orbiting M dwarfs AD Leo or GJ 463C, the CH_3Cl vertical mixing ratio profiles approximated isoprofiles up to at least 70 km in altitude. For such atmospheres, Segura *et al.* (2005) showed that CH_3Cl produces absorption features in the thermal IR near 7, 10, and 15 μm. Although Segura *et al.* (2005) did not simulate transit transmission spectra, the well-mixed profiles of CH_3Cl for the M dwarfs suggest it may be detectable in transit observations, even if such observations could only probe the upper layers of these atmospheres.

4.3. Interpretation of biosignatures in the planetary context

Generally speaking, it is important to consider any potential biosignature in the broader planetary context to rule out false-positive abiotic production mechanisms and search for other signs of habitability and life. Such additional constraints are important in all situations: the best understanding of any planet will come from a holistic consideration of many diverse pieces of information. The Solar System shows us that there is tremendous value in obtaining as much information as possible when interpreting difficult-to-access planetary characteristics. For example, the case for Europa's subsurface ocean was supported and strengthened by multiple lines of evidence ranging from surface morphology to Europa's induced magnetic field (*e.g.,* Squyres *et al.*, 1983; Carr *et al.*, 1998; Kivelson *et al.*, 2000; Stevenson, 2000).

Alarmingly, the nearby worlds in our solar system also have a rich history of misinterpretation in the absence of robust data. Percival Lowell's extensive analysis of the putative (and wholly illusionary) canals on Mars is perhaps the best-known example of this phenomenon (Lowell, 1906), but there are countless other less notorious cases. For instance, when G. Kuiper discovered Titan's atmosphere (Kuiper, 1944), he speculated that the moon's orange coloration is due to ''the action of the atmosphere on the surface itself, analogous to the oxidation supposed to be responsible for the orange color of Mars,'' not understanding that he was seeing the atmosphere rather than the planetary surface. Exoplanets, spatially unresolved and at vast distances, will be even more difficult to interpret. Because the designs of the first generation of observatories that include terrestrial exoplanet characterization and biosignature detection in their science goals are currently being studied, it is crucial that these design studies be informed by ongoing analyses of a variety of possible biosignatures, habitability signatures, and false positives of both. For these future observatories, a wide wavelength spectral range can mitigate the possibility of reaching erroneous conclusions by providing additional spectral context to consider any given feature. Additional context will be even more valuable when interpreting newly discovered planet types and characteristics not represented in the Solar System (*e.g.* hot Jupiters, mini-Neptunes, and super Earths). The diversity of planet types already discovered suggests that the probability of detecting a true Earth twin is very small, so it is crucial to expand our understanding of how habitability and biosignatures may appear on worlds different from the planet we live on. Somewhat paradoxically, we must do this before these exoplanets are even discovered; otherwise, we risk underdesigning the capabilities of the future observatories that will study them.

Organic haze is just one example of a potential novel biosignature. Haze itself is relatively simple to detect due to its strong spectral features, but as we have argued here, interpretation of haze spectral features will be challenging, dependent on several different pieces of information. Indeed, Titan's abiotic organic haze shows plainly that the detection of haze alone is inadequate for biosignature considerations. We have, in this study, discussed observing strategies to strengthen the case for a haze as biogenic: (1) When a haze is present in a sufficiently oxidizing background atmosphere, high methane fluxes may be required to produce it, and such high fluxes may suggest (but not prove) the involvement of biology, the most vigorous producer of methane on Earth today. (2) When a haze is present in an atmosphere that has less methane than photochemical models predict is required to initiate haze formation, this implies the existence of an additional hydrocarbon source like S_{org} gases. Beyond these two strategies, other measurements like the presence (or absence) of other biosignatures and habitability signatures like ocean glint (Robinson *et al.*, 2010, 2014) would provide valuable additional information that could strengthen (or weaken) the case for biological involvement.

Future work is necessary to more rigorously examine the rates of abiotic methane production that may be possible on other planet types and determine whether there are other abiotic mechanisms that generate hazes at unexpectedly low CH_4/CO_2 ratios. Additionally, as we emphasized above, future studies of other novel biosignatures and habitability signatures are also needed to expand our palette of known possible types of living planets. However, because photochemistry may generate non-intuitive or indirect spectral signs of these biological processes (*e.g.,* the spectral impacts of S_{org}), it is crucial for any considerations of novel spectral signatures to also include the context of the broader atmospheric and stellar flux environment.

4.4. False positives for organic haze

We considered several possible spectral mimics for organic haze in our previous study (Arney *et al.*, 2017). Given that the most detectable spectral signature of organic haze is its blue-UV absorption feature, other compounds with strong UV-blue absorption have the potential to be mistaken for organic haze. These include iron oxide, the unknown UV absorber in the venusian atmosphere, and exotic haze compounds such as zinc sulfide (ZnS, although its high condensation temperature means it is not a viable aerosol candidate for Earth-like atmospheres). An additional UV-blue-absorbing compound we did not consider in our previous study is S_8 particles, which can produce deep, broad blue-UV absorption features similar to organic haze when present in large quantities (Hu *et al.*, 2013). S_8 particles are produced by volcanic sulfur gas emissions; photochemical processing of these volcanic gases tends to favor production of H_2SO_4 aerosols under more oxidizing conditions, while S_8 is favored under more reducing conditions such as those that would also tend to generate organic haze (*e.g.,* Zahnle *et al,* 2006; Hu *et al.,* 2013). It may be possible to distinguish the spectral signatures of S_8 from organic haze via absorption features from emitted volcanic gases themselves (*e.g.,* H_2S and SO_2), but modeling work by Hu *et al.* (2013) shows these gases are photochemically short-lived, and their most detectable absorption features occur longward of 5 μm. This makes direct imaging detections of them very difficult—although transit observations probing to longer wavelengths may still be able to measure them. Organic haze produces its own diagnostic absorption features near 3 and 6 μm that may also be detectable in transit observations, allowing it to be distinguished from S_8 if IR transit observations are possible. We emphasize, again, as we did in Section 4.3, that any given spectral feature must be considered in the context of the whole planetary environment and with as much spectral contextual information as possible. A strong UV-blue wavelength absorber is more likely to be organic haze than S_8 particles if it is detected in the presence of strong CH_4 features, but if CH_4 features are weak or absent, S_8 (or other compounds like iron oxide) may be more likely. S_8 (and sulfate) concentrations may also be time-variable if volcanic outbursts occur sporadically, and time-resolved spectroscopy may be a powerful means of identifying false positives of volcanic emissions (Misra *et al.*, 2015).

5. Conclusions

Organic haze formation on Archean Earth was likely controlled by biological methane production, and this type of haze may also occur on anoxic worlds elsewhere. On planets with Archean-like CO_2 levels, organic haze formation requires methane production consistent with known and theoretical biological fluxes on Earth. However, because abiotic processes can also produce methane, methods to distinguish biotic and abiotic hazes are needed. To that end, we explored how biogenic organic sulfur gases affect haze formation since these gases can liberate methyl radicals that become involved in haze production. We find organic sulfur gases can drive haze formation at lower CH_4/CO_2 ratios compared to methane photochemistry alone. This effect is especially pronounced around M dwarfs with lower UV fluxes than the Sun. To make the case for a S_{org}-mediated haze impacting a planet's spectrum, it will be necessary to constrain the atmospheric CH_4/CO_2 ratio to test whether the haze is present at an anomalously low ratio unexplainable by methane photochemistry alone. Although S_{org} gases themselves are difficult to detect in a planet's spectrum, organic haze produces a very strong absorption feature at UV-blue wavelengths. This haze could also be detected in the NIR and mid-IR by transit transmission observations. Methane and carbon dioxide produce absorption features in the NIR that could be detected in both reflected light and transit transmission observations. Future observatories and telescope concepts such as JWST, LUVOIR, and HabEx may be able to make measurements of these spectral features. Because the haze absorption feature is so strong, it may be one of the most detectable spectral beacons of life, although interpreting the haze absorption feature in the context of its environment may be more challenging. The long anoxic history of our planet teaches us not to ignore the challenge of life detection on anoxic worlds when we design the instruments, plan the observations, and search for life on distant exoplanets.

Acknowledgments

This work was performed as part of the NASA Astrobiology Institute's Virtual Planetary Laboratory, supported by the National Aeronautics and Space Administration through the NASA Astrobiology Institute under solicitation NNH12ZDA002C and Cooperative Agreement Number NNA13AA93A. Simulations were facilitated through the use of the Hyak supercomputer system at the University of Washington eScience Institute. We thank Dr. T. McCollom for pointing us to sources discussing methane in serpentinizing systems. Spectra shown in this work will be archived at the Virtual Planetary Laboratory online spectral database. We thank our two anonymous reviewers for their helpful comments and suggestions that improved our manuscript.

Author Disclosure Statement

No competing financial interests exist.

References

Allen, M., Pinto, J.P., and Yung, Y.L. (1980) Titan: aerosol photochemistry and variations related to the sunspot cycle. *Astrophys J* 242:L125–L128.

Anbar, A.D., Yung, Y.L., and Chavez, F.P. (1996) Methyl bromide: ocean sources, ocean sinks, and climate sensitivity. *Global Biogeochem Cycles* 10:175–190.

Arney, G., Domagal-Goldman, S.D., Meadows, V.S., Wolf, E.T., Schwieterman, E., Charnay, B., Claire, M., Hébrard, E., and Trainer, M.G. (2016) The pale orange dot: the spectrum and habitability of hazy Archean Earth. *Astrobiology* 16:873–899.

Arney, G.N., Meadows, V.S., Domagal-Goldman, S.D., Deming, D., Robinson, T.D., Tovar, G., Wolf, E.T., and Schwieterman, E. (2017) Pale orange dots: the impact of organic haze on the habitability and detectability of Earthlike exoplanets. *Astrophys J* 836, doi:10.3847/1538-4357/836/1/49.

Beichman, C., Benneke, B., Knutson, H., Smith, R., Lagage, P.-O., Dressing, C., Latham, D., Lunine, J., Birkmann, S., Ferruit, P., Giardino, G., Kempton, E., Carey, S., Krick, J., Deroo, P.D., Mandell, A., Ressler, M.E., Shporer, A., Swain, M., Vasisht, G., Ricker, G., Bouwman, J., Crossfield, I., Greene, T., Howell, S., Christiansen, J., Ciardi, D., Clampin, M., Greenhouse, M., Sozzetti, A., Goudfrooij, P., Hines, D., Keyes, T., Lee, J., McCullough, P., Robberto, M., Stansberry, J., Valenti, J., Rieke, M., Rieke, G., Fortney, J., Bean, J., Kreidberg, L., Ehrenreich, D., Deming, D., Albert, L., Doyon, R., and Sing, D. (2014) Observations of transiting exoplanets with the James Webb Space Telescope (JWST). *Publ Astron Soc Pac* 126:1134–1173.

Blake, N., Blake, D.R., Sive, B.C., Chen, T., Sherwood Rowland, F., Collins, J.E.J., Sachse, G.W., and Anderson, B.E. (1996) Biomass burning emissions and vertical distribution of atmospheric methyl halides and other reduced carbon gases in the South Atlantic region. *J Geophys Res: Atmospheres* 101: 24151–24164.

Bolcar, M.R., Balasubramanian, K., Clampin, M., Crooke, J., Feinberg, L., Postman, M., Quijada, M., Rauscher, B., Redding, D., Rioux, N., Shaklan, S., Stahl, H.P., Stahle, C., and Thronson, H. (2015) Technology development for the Advanced Technology Large Aperture Space Telescope (ATLAST) as a candidate Large UV-Optical-Infrared (LUVOIR) surveyor. *Proc SPIE* 9602, doi:10.1117/12.2188559.

Botet, R., Rannou, P., and Cabane, M. (1997) Mean-field approximation of Mie scattering by fractal aggregates of identical spheres. *Appl Opt* 36:8791–8797.

Bradley, A.S. and Summons, R.E. (2010) Multiple origins of methane at the Lost City hydrothermal field. *Earth Planet Sci Lett* 297:34–41.

Brazelton, W.J., Schrenk, M.O., Kelley, D.S., and Baross, J.A. (2006) Methane- and sulfur-metabolizing microbial communities dominate the Lost City hydrothermal field ecosystem. *Appl Environ Microbiol* 72:6257–6270.

Carr, M.H., Belton, M.J.S., Chapman, C.R., Davies, M.E., Geissler, P., Greenberg, R., McEwen, A.S., Tufts, B.R., Greeley, R., Sullivan, R., Head, J.W., Pappalardo, R.T., Klaasen, K.P., Johnson, T.V., Kaufman, J., Senske, D., Moore, J., Neukum, G., Schubert, G., Burns, J.A., Thomas, P., and Veverka, J. (1998) Evidence for a subsurface ocean on Europa. *Nature* 391:363–365.

Claire, M.W., Sheets, J., Cohen, M., Ribas, I., Meadows, V.S., and Catling, D.C. (2012) The evolution of solar flux from 0.1 nm to 160 μm: quantative estimates for planetary studies. *Astrophys J* 757, doi:10.1088/0004-637X/757/1/95.

Claire, M.W., Kasting, J.F., Domagal-Goldman, S.D., Stüeken, E.E., Buick, R., and Meadows, V.S (2014) Modeling the signature of sulfur mass-independent fractionation produced in the Archean atmosphere. *Geochim Cosmochim Acta* 141: 365–380.

Core Writing Team, Pachauri, R.K., and Reisinger, A., editors. (2007) *Climate Change 2007: Synthesis Report,* Contribution of Working Groups I, II and III to the fourth assessment report of the Intergovernmental Panel on Climate Change, IPCC, Geneva, Switzerland.

Crisp, D. (1997) Absorption of sunlight by water vapor in cloudy conditions: a partial explanation for the cloud absorption anomaly. *Geophys Res Lett* 24:571–574.

Dalcanton, J., Seager, S., Aigrain, S., Hirata, C., Battel, S., Mather, J., Brandt, N., Postman, M., Conroy, C., Redding, D., and Feinberg, L. (2015) *From Cosmic Birth to Living Earths: the Future of UVOIR Space Astronomy,* Association of Universities for Research in Astronomy, Washington, DC.

Dauphas, N. and Kasting, J.F. (2011) Low pCO_2 in the pore water, not in the Archean air. *Nature* 474, doi:10.1038/nature09960.

DeWitt, H.L., Trainer, M.G., Pavlov, A.A., Hasenkopf, C.A., Aiken, A.C., Jimenez, J.L., McKay, C.P., Toon, O.B., and Tolbert, M.A. (2009) Reduction in haze formation rate on prebiotic Earth in the presence of hydrogen. *Astrobiology* 9: 447–453.

Domagal-Goldman, S.D., Kasting, J.F., Johnston, D.T., and Farquhar, J. (2008) Organic haze, glaciations and multiple sulfur isotopes in the Mid-Archean era. *Earth Planet Sci Lett* 269:29–40.

Domagal-Goldman, S.D., Meadows, V.S., Claire, M.W., and Kasting, J.F. (2011) Using biogenic sulfur gases as remotely detectable biosignatures on anoxic planets. *Astrobiology* 11: 419–441.

Domagal-Goldman, S.D., Segura, A., Claire, M.W., Robinson, T.D., and Meadows, V.S. (2014) Abiotic ozone and oxygen in atmospheres similar to prebiotic Earth. *Astrophys J* 792, doi: 10.1088/0004-637X/792/2/90.

Driese, S.G., Jirsa, M.A., Ren, M., Brantley, S.L., Sheldon, N.D., Parker, D., and Schmitz, M. (2011) Neoarchean paleoweathering of tonalite and metabasalt: implications for reconstructions of 2.69 Ga early terrestrial ecosystems and paleoatmospheric chemistry. *Precambrian Res* 189:1–17.

Emmanuel, S. and Ague, J.J. (2007) Implications of present-day abiogenic methane fluxes for the early Archean atmosphere. *Geophys Res Lett* 34, doi:10.1029/2007GL030532.

Etiope, G. (2012) Climate science: methane uncovered. *Nat Geosci* 5:373–374.

Etiope, G. and Sherwood Lollar, B. (2013) Abiotic methane on Earth. *Rev Geophys* 51:276–299.

Etiope, G., Fridriksson, T., Italiano, F., Winiwarter, W., and Theloke, J. (2007) Natural emissions of methane from geothermal and volcanic sources in Europe. *Journal of Volcanology and Geothermal Research* 165:76–86.

France, K., Linsky, J.L., Tian, F., Froning, C.S., and Roberge, A. (2012) Time-resolved ultraviolet spectroscopy of the M-dwarf GJ 876 exoplanetary system. *Astrophys J* 750:L32.

Guzmán-Marmolejo, A., Segura, A., and Escobar-Briones, E. (2013) Abiotic production of methane in terrestrial planets. *Astrobiology* 13:550–559.

Haqq-Misra, J.D., Domagal-Goldman, S.D., Kasting, P.J., and Kasting, J.F. (2008) A revised, hazy methane greenhouse for the Archean Earth. *Astrobiology* 8:1127–1137.

Harman, C.E., Schwieterman, E.W., Schottelkotte, J.C., and Kasting, J.F. (2015) Abiotic O_2 levels on planets around F, G, K, and M stars: possible false positives for life? *Astrophys J* 812, doi:10.1088/0004-637X/812/2/137.

Harper, D., Hamilton, J.T., Ducrocq, V., Kennedy, J.T., Downey, A., and Kalin, R.M. (2003) The distinctive isotopic signature of plant-derived chloromethane: possible application in constraining the atmospheric chloromethane budget. *Chemosphere* 52:433–436.

Hasenkopf, C.A., Beaver, M.R., Trainer, M.G., Langley Dewitt, H., Freedman, M.A., Toon, O.B., McKay, C.P., and Tolbert, M.A. (2010) Optical properties of Titan and early Earth haze laboratory analogs in the mid-visible. *Icarus* 207:903–913.

Hasenkopf, C.A., Freedman, M.A., Beaver, M.R., Toon, O.B., and Tolbert, M.A. (2011) Potential climatic impact of organic haze on early Earth. *Astrobiology* 11:135–149.

Hicks, R.K., Day, D.A., Jimenez, J.L., and Tolbert, M.A. (2016) Follow the carbon: isotopic labeling studies of early Earth aerosol. *Astrobiology* 16:822–830.

Hörst, S.M. and Tolbert, M.A. (2014) The effect of carbon monoxide on planetary haze formation. *Astrophys J* 781, doi: 10.1088/0004-637X/781/1/53.

Hu, R., Seager, S., and Bains, W. (2013) Photochemistry in terresrial exoplanet atmospheres. II. H_2S and SO_2 photochemimstry in anoxic atmospheres. *Astrophys J* 769, doi: 10.1088/0004-637X/769/1/6.

Izon, G., Zerkle, A.L., Zhelezinskaia, I., Farquhar, J., Newton, R.J., Poulton, S.W., Eigenbrode, J.L., and Claire, M.W. (2015) Multiple oscillations in Neoarchaean atmospheric chemistry. *Earth Planet Sci Lett* 431:264–273.

Izon, G., Zerkle, A.L., Williford, K.H., Farquhar, J., Poulton, S.W., and Claire, M.W. (2017) Biological regulation of atmospheric chemistry en route to planetary oxygenation. *Proc Natl Acad Sci USA* 114:E2571–E2579.

Kanzaki, Y. and Murakami, T. (2015) Estimates of atmospheric CO_2 in the Neoarchean–Paleoproterozoic from paleosols. *Geochim Cosmochim Acta* 159:190–219.

Kasting, J. and Ackerman, T. (1986) Climactic consequences of very high carbon dioxide levels in the Earth's early atmosphere. *Science* 234:1383–1385.

Kasting, J.F. (2005) Methane and climate during the Precambrian era. *Precambrian Res* 137:119–129.

Kasting, J.F. and Catling, D. (2003) Evolution of a habitable planet. *Annu Rev Astron Astrophys* 41:429–463.

Kasting, J.F., Liu, S.C., and Donahue, T.M. (1979) Oxygen levels in the prebiological atmosphere. *J Geophys Res* 84: 3097–3207.

Kelley, D.S., Karson, J.A., Fru, G.L., Yoerger, D.R., Shank, T.M., Butterfield, D.A., Hayes, J.M., Schrenk, M.O., Olson, E.J., Proskurowski, G., Jakuba, M., Bradley, A., Larson, B., Ludwig, K., Glickson, D., Buckman, K., Bradley, A.S., Brazelton, W.J., Roe, K., Elend, M.J., Delacour, A., Bernasconi, S.M., Lilley, M.D., Baross, J.A., Summons, R.E., and Sylva, S.P. (2005) A serpentinite-hosted ecosystem: the Lost City hydrothermal field. *Science* 307:1428–1434.

Keppler, F., Eiden, R., Niedan, V., Pracht, J., and Scholer, H.F. (2000) Halocarbons produced by natural oxidation processes during degradation of organic matter. *Nature* 403:298–301.

Keppler, F., Harper, D.B., Röckmann, T., Moore, R.M., and Hamilton, J.T.G. (2005) New insight into the atmospheric chloromethane budget gained using stable carbon isotope ratios. *Atmos Chem Phys Discuss* 5:3899–3919.

Kerrich, R. and Polat, A. (2006) Archean greenstone-tonalite duality: thermochemical mantle convection models or plate tectonics in the early Earth global dynamics? *Tectonophysics* 415:141–165.

Kestler, D.P., Mayne, B.C., Ray, T.B., Goldstein, L.D., Brown, R.H., and Black, C.C. (1975) Biochemical components of the photosynthetic CO_2 compensation point of higher plants. *Biochem Biophys Res Commun* 66:1439–1446.

Khare, B.N., Sagan, C., Arakawa, E.T., Suits, F., Callcott, T.A., and Williams, M.W. (1984) Optical constants of organic tholins produced in a simulated titanian atmosphere: from soft X-ray to microwave frequencies. *Icarus* 60:127–137.

Kharecha, P., Kasting, J., and Siefert, J. (2005) A coupled atmosphere-ecosystem model of the early Archean Earth. *Geobiology* 3:53–76.

Kivelson, M.G., Khurana, K.K., Russell, C.T., Volwerk, M., Walker, R.J., and Zimmer, C. (2000) Galileo magnetometer measurements: a stronger case for a subsurface ocean at Europa. *Science* 289:1340–1343.

Kopparapu, R.K., Ramirez, R., Kasting, J.F., Eymet, V., Robinson, T.D., Mahadevan, S., Terrien, R.C., Domagal-Goldman, S., Meadows, V., and Deshpande, R. (2013) Habitable zones around main-sequence stars: new estimates. *Astrophys J* 765, doi10.1088/0004-637X/765/2/131.

Koppmann, R., Johen, F.J., Plass-Dulmer, C., and Rudolph, J. (1993) Distribution of methylchloride, dichloromethane, trichloroethene and tetrachloroethene over the North and South Atlantic. *J Geophys Res: Atmospheres* 98:20517–20526.

Kuiper, G. (1944) Titan: a satellite with an atmosphere. *Astrophys J* 100:378.

Kurzweil, F., Claire, M., Thomazo, C., Peters, M., Hannington, M., and Strauss, H. (2013) Atmospheric sulfur rearrangement 2.7 billion years ago: evidence for oxygenic photosynthesis. *Earth Planet Sci Lett* 366:17–26.

Lomans, B.P., van der Drift, C., Pol, A., and Op den Camp, H.J. (2002) Microbial cycling of volatile organic sulfur compounds. *Cell Mol Life Sci* 59:575–588.

López-Puertas, M., Dinelli, B.M., Adriani, A., Funke, B., García-Comas, M., Moriconi, M.L., D'Aversa, E., Boersma, C., and Allamandola, L.J. (2013) Large abundances of polycyclic aromatic hydrocarbons in Titan's upper atmosphere. *Astrophys J* 770, doi:10.1088/0004-637X/770/2/132.

Lowell, P. (1906) *Mars and Its Canals,* The Macmillan Company, London.

Luger, R. and Barnes, R. (2015) Extreme water loss and abiotic O_2 buildup on planets. *Astrobiology* 15:119–143.

Lupu, R., Marley, M., Lewis, N., Line, M., Traub, W., and Zahnle, K. (2016) Developing atmospheric retrieval methods for direct imaging spectroscopy of gas giants in reflected light. I. Methane abundances and basic cloud properties. *Astron J* 152, doi:10.3847/0004-6256/152/6/217.

Manley, S.L. and Dastoor, M.N. (1988) Methyl iodide (CH_3I) production by kelp and associated microbes. *Mar Biol* 98: 477–482.

McCauley, S.E., Goldstein, A.H., and DePaolo, D.J. (1999) An isotopic approach for understanding the CH_3Br budget of the atmosphere. *Proc Natl Acad Sci USA* 96:10006–10009.

McCollom, T.M. (2016) Abiotic methane formation during experimental serpentinization of olivine. *Proc Natl Acad Sci USA* 113:13965–13970.

McDermott, J.M., Seewald, J.S., German, C.R., and Sylva, S.P. (2015) Pathways for abiotic organic synthesis at submarine hydrothermal fields. *Proc Natl Acad Sci USA* 112:7668–7672.

Meadows, V. and Crisp, D. (1996) Ground-based near-infrared observations of the Venus nightside? The thermal structure and water abundance near the surface. *J Geophys Res: Planets* 101:4595–4622.

Mennesson, B., Gaudi, S., Seager, S., Cahoy, K., Domagal-Goldman, S., Feinberg, L., Guyon, O., Kasdin, J., Marois, C., Mawet, D., Tamura, M., Mouillet, D., Prusti, T., Quirrenbach, A., Robinson, T., Rogers, L., Scowen, P., Somerville, R., Stapelfeldt, K., Stern, D., Still, M., Turnbull, M., Booth, J., Kiessling, A., Kuan, G., and Warfield, K. (2016) The Habitable Exoplanet (HabEx) imaging mission: preliminary science drivers and technical requirements. *Proc SPIE* 9904, doi:10.1117/12.2240457.

Misra, A., Meadows, V., Claire, M., and Crisp, D. (2014a) Using dimers to measure biosignatures and atmospheric pressure for terrestrial exoplanets. *Astrobiology* 14:67–86.

Misra, A., Meadows, V., and Crisp, D. (2014b) The effects of refraction on transit transmission spectroscopy: application to Earth-like exoplanets. *Astrophys J* 792, doi:10.1088/0004-637X/792/1/61.

Misra, A., Krissansen-Totton, J., Koehler, M.C., and Sholes, S. (2015) Transient sulfate aerosols as a signature of exoplanet volcanism. *Astrobiology* 15:462–477.

Moran, J.J., House, C.H., Vrentas, J.M., and Freeman, K.H. (2008) Methyl sulfide production by a novel carbon monoxide metabolism in *Methanosarcina acetivorans*. *Appl Environ Microbiol* 74:540–542.

Nayak, M., Roxana, L., Marley, M., Fortney, J., Robinson, T., and Lewis, N. (2017) Atmospheric retrieval for direct imaging spectroscopy of gas giants in reflected light. II. Orbital phase and planetary radius. *Publ Astron Soc Pac* 129, doi:10.1088/1538-3873/129/973/034401.

Pare, P.W. and Tumlinson, J.H. (1999) Update on plant-insect interactions: plant volatiles as a defense against insect herbivores. *Plant Physiol* 121:325–331.

Pavlov, A., Brown, L., and Kasting, J. (2001a) UV shielding of NH_3 and O_2 by organic hazes in the Archean atmosphere. *J Geophys Res* 106:23267–23287.

Pavlov, A., Kasting, J., Eigenbrode, J., and Freeman, K. (2001b) Organic haze in Earth's early atmosphere: source of low-^{13}C Late Archean kerogens? *Geology* 29:1003–1006.

Pilcher, C. (2003) Biosignatures of early Earths. *Astrobiology* 3:471–486.

Planavsky, N.J., Reinhard, C.T., Wang, X., Thomson, D., McGoldrick, P., Rainbird, R.H., … and Lyons, T.W. (2014) Low Mid-Proterozoic atmospheric oxygen levels and the delayed rise of animals. *Science* 346: 635–638.

Postman, M., Traub, W., Krist, J., Stapelfeldt, K., Brown, R., Oegerle, W., Lo, A., Clampin, M., Soummer, R., Wiseman, J., and Mountain, M. (2010) Advanced Technology Large-Aperture Space Telescope (ATLAST): characterizing habitable worlds. *ASP Conference Series* 430:361–367.

Rannou, P., Cabane, M., Botet, R., and Chassèfiere, E. (1997) A new interpretation of scattered light measurements at Titan's limb. *J Geophys Res* 102:10997–11013.

Rasmussen, R.A., Khalili, M.A.K., Gunawardena, R., and Hoyt, S.D. (1982) Atmospheric methyl iodide (CH_3I). *J Geophys Res: Oceans* 87:3086–3090.

Rhew, R. (2011) Sources and sinks of methyl bromide and methyl chloride in the tallgrass prairie: applying a stable isotope tracer technique over highly variable gross fluxes. *J Geophys Res: Biogeosciences* 116, doi:10.1029/2011JG001704.

Robinson, T.D., Meadows, V.S., and Crisp, D. (2010) Detecting oceans on extrasolar planets using the glint effect. *Astrophys J* 721:L67–L71.

Robinson, T.D., Meadows, V.S., Crisp, D., Deming, D., A'hearn, M.F., Charbonneau, D., Livengood, T.A., Seager, S., Barry, R.K., Hearty, T., Hewagama, T., Lisse, C.M., McFadden, L.A., and Wellnitz, D.D. (2011) Earth as an extrasolar planet: Earth model validation using EPOXI earth observations. *Astrobiology* 11:393–408.

Robinson, T.D., Ennico, K., Meadows, V.S., Sparks, W., Bussey, D.B.J., Schwieterman, E.W., and Breiner, J. (2014) Detection of ocean glint and ozone absorption using LCROSS Earth observations. *Astrophys J* 787, doi:10.1088/0004-637X/787/2/171.

Robinson, T.D., Stapelfeldt, K.R., and Marley, M.S. (2016) Characterizing rocky and gaseous exoplanets with 2-meter class space-based coronagraphs. *Publ Astron Soc Pac* 128, doi:10.1088/1538-3873/128/960/025003.

Rosing, M.T., Bird, D.K., Sleep, N.H., and Bjerrum, C.J. (2010) No climate paradox under the faint early Sun. *Nature* 464:744–747.

Rothman, L.S., Gordon, I.E., Babikov, Y., Barbe, A., Chris Benner, D., Bernath, P.F., Birk, M., Bizzocchi, L., Boudon, V., Brown, L.R., Campargue, A., Chance, K., Cohen, E.A., Coudert, L.H., Devi, V.M., Drouin, B.J., Fayt, A., Flaud, J.-M., Gamache, R.R., Harrison, J.J., Hartmann, J.-M., Hill, C., Hodges, J.T., Jacquemart, D., Jolly, A., Lamouroux, J., LeRoy, R.J., Li, G., Long, D.A., Lyulin, O.M., Mackie, C.J., Massie, S.T., Mikhailenko, S., Müller, H.S.P., Naumenko, O.V., Nikitin, A.V., Orphal, J., Perevalov, V., Perrin, A., Polovtseva, E.R., Richard, C., Smith, M.A.H., Starikova, E., Sung, K., Tashkun, S., Tennyson, J., Toon, G.C., Tyuterev, Vl.G., and Wagner, G. (2013) The HITRAN2012 molecular spectroscopic database. *J Quant Spectrosc Radiat Transf* 130:4–50.

Sagan, C. and Chyba, C. (1997) The early faint young Sun paradox: organic shielding of ultraviolet-labile greenhouse gases. *Science* 276:1217–1221.

Schwieterman, E.W., Meadows, V.S., Domagal-Goldman, S.D., Deming, D., Arney, G.N., Luger, R., Harman, C.E., Misra, A., and Barnes, R. (2016) Identifying planetary biosignature impostors: spectral features of CO and O_4 resulting from abiotic O_2/O_3 production. *Astrophys J* 819, doi:10.3847/2041-8205/819/1/L13.

Seager, S., Schrenk, M., and Bains, W. (2012) An astrophysical view of Earth-based metabolic biosignature gases. *Astrobiology* 12:61–82.

Segura, A., Kasting, J.F., Meadows, V., Cohen, M., Scalo, J., Crisp, D., Butler, R.A.H., and Tinetti, G. (2005) Biosignatures from Earth-like planets around M dwarfs. *Astrobiology* 5:706–725.

Shaw, G.H. (2008) Earth's atmosphere—Hadean to early Proterozoic. *Chemie der Erde - Geochemistry* 68:235–264.

Sive, B.C., Varner, R.K., Mao, H., Blake, D.R., Wingenter, O.W., and Talbot, R. (2007) A large terrestrial source of methyl iodide. *Geophys Res Lett* 34:6–10.

Solomon, S.J., Custer, T., Schade, G., Soares Dias, A.P., and Burrows, J. (2005) Atmospheric methanol measurement using selective catalytic methanol to formaldehyde conversion. *Atmos Chem Phys Discuss* 5:3533–3559.

Squyres, S.W., Reynolds, R.T., Cassen, P.M., and Peale, S.J. (1983) Liquid water and active resurfacing on Europa. *Nature* 301:225–226.

Stapelfeldt, K.R., Dekens, F.G., Brenner, M.P., Warfield, K.R., Belikov, R., Brugarolas, P.B., Bryden, G., Cahoy, K.L., Chakrabarti, S., Dubovitsky, S., Effinger, R.T., Hirsch, B., Kissil, A., Krist, J.E., Lang, J.J., Marley, M.S., McElwain, M.W., Meadows, V.S., Nissen, J., Oseas, J.M., Pong, C., Serabyn, E., Sunada, E., Trauger, J.T., and Unwin, S.C. (2015) Exo-C: a probe-scale space observatory for direct imaging and spectroscopy of extrasolar planetary systems. *Proc SPIE* 9605, doi:10.1117/12.2191720.

Stevenson, D. (2000) Europa's ocean—the case strengthens. *Science* 289:1305–1307.

Stoner, D.L., Burbank, N.S., and Miller, K.S. (1994) Anaerobic transformation of organosulfur compounds in microbial mats from Octopus Spring. *Geomicrobiology* 12:195–202.

Tolbert, N.E., Benker, C., and Beck, E. (1995) The oxygen and carbon dioxide compensation points of C3 plants: possible role in regulating atmospheric oxygen. *Proc Natl Acad Sci USA* 92:11230–11233.
Trainer, M.G., Pavlov, A.A., DeWitt, H.L., Jimenez, J.L., McKay, C.P., Toon, O.B., and Tolbert, M.A. (2006) Organic haze on Titan and the early Earth. *Proc Natl Acad Sci USA* 103:18035–18042.
Turnbull, M.C., Glassman, T., Roberge, A., Cash, W., Noecker, C., Lo, A., Mason, B., Oakley, P., and Bally, J. (2012) The search for habitable worlds. 1. The viability of a starshade mission. *Publ Astron Soc Pac* 124, doi:10.1086/666325.
Ueno, Y., Yamada, K., Yoshida, N., Maruyama, S., and Isozaki, Y. (2006) Evidence from fluid inclusions for microbial methanogenesis in the early Archaean era. *Nature* 440:516–519.
Vance, S., Christensen, L.E., Webster, C.R., and Sung, K. (2011) Volatile organic sulfur compounds as biomarkers complementary to methane: infrared absorption spectroscopy of CH_3SH enables *in situ* measurements on Earth and Mars. *Planet Space Sci* 59:299–303.
Ver Eecke, H.C., Butterfield, D.A., Huber, J.A., Lilley, M.D., Olson, E.J., Roe, K.K., Evans, L.J., Merkel, A.Y., Cantin, H.V., and Holden, J.F. (2012) Hydrogen-limited growth of hyperthermophilic methanogens at deep-sea hydrothermal vents. *Proc Natl Acad Sci USA* 109:13674–13679.
Von Braun, K., Boyajian, T.S., van Belle, G.T., Kane, S.R., Jones, J., Farrington, C., Schaefer, G., Vargas, N., Scott, N., ten Brummelaar, T.A., Kephart, M., Gies, D.R., Ciardi, D.R., Lopez-Morales, M., Mazingue, C., McAlister, H.A., Ridgway, S., Goldfinger, P.J., Turner, N.H., and Sturmann, L. (2014) Stellar diameters and temperatures—V. 11 newly characterized exoplanet host stars. *Mon Not R Astron Soc* 438:2413–2425.
Vuitton, V., Tran, B.N., Persans, P.D., and Ferris, J.P. (2009) Determination of the complex refractive indices of Titan haze analogs using photothermal deflection spectroscopy. *Icarus* 203:663–671.
Waite, J.H., Young, D.T., Cravens, T.E., Coates, A.J., Crary, F.J., Magee, B., and Westlake, J. (2007) The process of tholin formation in Titan's upper atmosphere. *Science* 316: 870–875.
Walser, M.L., Park, J., Gomez, A.L., Russell, A.R., and Nizkorodov, S.A. (2007) Photochemical aging of secondary organic aerosol particles generated from the oxidation of d-limonene. *J Phys Chem A* 111:1907–1913.
Went, F.W. (1960) Blue hazes in the atmosphere. *Nature* 187: 641–643.
Woese, C.R. and Fox, G.E. (1977) Phylogenetic structure of the prokaryotic domain: the primary kingdoms. *Proc Natl Acad Sci USA* 74:5088–5090.
Wolf, E.T. and Toon, O.B. (2010) Fractal organic hazes provided an ultraviolet shield for early Earth. *Science* 328:1266–1268.
Xin, J.-Y., Cui, J., Niu, J., Hua, S., Xia, C., and Li, S. (2004) Production of methanol from methane by methanotrophic bacteria. *Biocatal Biotransformation* 22:225–229.
Yokouchi, Y., Noijiri, Y., Barrie, L.A., Toom-Sauntry, D., Machida, T., Inuzuka, Y., Akimoto, H., Li, H.J., Fujinuma, Y., and Aoki, S. (2000) A strong source of methyl chloride to the atmosphere from tropical coastal land. *Nature* 403:295–298.
Yung, Y.L., Allen, M., and Pinto, J.P. (1984) Photochemistry of the atmosphere of Titan: comparison between model and observations. *Astrophys J Suppl Ser* 55:465–506.
Zahnle, K., Claire, M., and Catling, D. (2006) The loss of mass-independent fractionation in sulfur due to a Palaeoproterozoic collapse of atmospheric methane. *Geobiology* 4:271–283.
Zerkle, A.L., Claire, M.W., Domagal-Goldman, S.D., Farquhar, J., and Poulton, S.W. (2012) A bistable organic-rich atmosphere on the Neoarchaean Earth. *Nat Geosci* 5:359–363.

Address correspondence to:
Giada Arney
NASA Goddard Space Flight Center
Mail Code 693
8800 Greenbelt Road
Greenbelt, MD 20771

E-mail: giada.n.arney@nasa.gov

Submitted 8 March 2017
Accepted 20 September 2017

Abbreviations Used

HabEx = Habitable Exoplanet Imaging Mission
IWA = inner working angle
JWST = James Webb Space Telescope
LUVOIR = Large UV Optical Infrared telescope
NIR = near infrared
SMART = Spectral Mapping Atmospheric Radiative Transfer model
SNR = signal-to-noise ratio